Journal of Chemical Technology and Biotechnology SCI

Dynamic Process Modeling and Hybrid Intelligent Control of Ethylene Copolymerization in Gas-phase Catalytic Fluidized-bed Reactors

Journal:	*Journal of Chemical Technology & Biotechnology*
Manuscript ID	JCTB-18-1397.R1
Wiley - Manuscript type:	Research Article
Date Submitted by the Author:	n/a
Complete List of Authors:	Abbasi, Mohammad Reza; University of Malaya, Department of Chemical Engineering Shamiri, Ahmad; Rapid and Professional Industrial Development and Service Pty. Ltd., Main department Hussain, Mohd Azlan; Universiti Malaya, Chemical Engineering Aghay Kaboli, Seyed Hamidreza; University of Malaya - City Campus, University of Malaya Power Energy Dedicated Advanced Centre (UMPEDAC)
Key Words:	Catalytic Processes, Catalytic Reactors, Control, Dynamics, Heterogeneous Catalysis, Modelling

Dynamic Process Modeling and Hybrid Intelligent Control of Ethylene Copolymerization in Gas-phase Catalytic Fluidized-bed Reactors

Mohammad Reza Abbasi[a], *Ahmad Shamiri*[b,c,*], *Mohamed Azlan Hussain*[a,*], *Seyed Hamidreza Aghay Kaboli*[d]

[a] *Department of Chemical Engineering, Faculty of Engineering, University of Malaya, 50603 Kuala Lumpur, Malaysia*
[b] *Rapid and Professional Industrial Development and Service Pty. Ltd., Lucy Court, Bundoora, VIC 3083, Australia*
[c] *Chemical & Petroleum Engineering Department, Faculty of Engineering, Technology & Built Environment, UCSI University, 56000 Kuala Lumpur, Malaysia*
[d] *University of Malaya Power Energy Dedicated Advanced Centre (UMPEDAC), Wisma R&D University Malaya (UM), Jalan Pantai Baharu, 59990, Kuala Lumpur, Malaysia*

ABSTRACT

BACKGROUND: Polyethylene (PE) is the most extensively consumed plastic in the world and gas-phase based processes are widely used for its production due to their flexibility. The sole type of reactor that can produce PE in gas-phase is fluidized bed reactor (FBR) and effective modeling and control of FBRs are of great importance for design, scale-up and simulation studies. This paper discusses these issues and suggests a novel advance control structure for these systems.

RESULTS: A unified process modeling and control approach is introduced for ethylene copolymerization in FBRs. The results show that our previously developed two-phase model is well confirmed using real industrial data and is exact enough to further develop different control strategies. It is also shown that due to high system nonlinearities, conventional controllers are not suitable for this system and advance controllers are needed for this system. Melt flow index (MFI) and reactor temperature are chosen as vital variables and intelligent controllers were able to sufficiently control them. Performance indicators show that advanced controllers have a superior performance in comparison with conventional controllers.

CONCLUSION: Based on control performance indicators, the adaptive neuro-fuzzy inference system (ANFIS) controller for MFI control and the hybrid ANFIS-PID controller for temperature control perform better regarding the disturbance rejection and set point tracking in comparison with the conventional controllers.

Keywords: *Polyethylene; Process control; Fluidized-Bed Reactor; Dynamic Modeling; Solid Elutriation; Artificial Intelligence*
Short Title: Dynamic Modeling and Advanced Control of Ethylene Copolymerization in FBRs
Declarations of interest: none

* Corresponding author: Tel.: +60 379675214, fax: +60 379675319 (M. A. Hussain)
Email addresses: m_abbasi@ifac-mail.org (Mohammad Reza Abbasi), ahmadshamiri@gmail.com (Ahmad Shamiri), kaboli@siswa.um.edu.my (Seyed Hamidreza Aghay Kaboli), mohd_azlan@um.edu.my (Mohamed Azlan Hussain)

NOMENCLATURE

A	cross sectional area of the reactor (m^2)	M_n	number average molecular weight of polymer (kg/kmol)
ALDMC	adaptive linear DMC	MPC	model predictive controller
AI	artificial intelligence	M_w	weight average molecular weight of polymer (kg/kmol)
$AlEt_3$	triethyl aluminum co-catalyst	MWD	molecular weight distribution
ANFIS	adaptive neuro-fuzzy inference system	mw_i	molecular weight of monomer i (g/mol)
APMBC	adaptive Predictive Model-Based Control	N(0, j)	uninitiated site of type j produced by formation reaction
Ar	Archimedes number	NARMAX	Nonlinear Auto Regressive Moving Average with eXogenous input
B_i	moles of reacted monomer bound in the polymer in the reactor	$N^*(j)$	potential active site of type j
CFD	computational fluid dynamics	$N_d(j)$	spontaneously deactivated site of type j
$C_{p,pol}$	specific heat capacity of solid product (J/kg·K)	$N_{dIH}(0, j)$	impurity killed sites of type j
C_{pg}	specific heat capacity of gaseous stream (J/kg·K)	N_H	uninitiated site of type j produced by transfer to hydrogen reaction
C_{pi}	specific heat capacity of component i (J/kg·K)	$N_j(r, j)$	living polymer molecule of length r, growing at an active site of type j, with terminal monomer M
CSTR	continuous stirred tank reactor	P	pressure (Pa)
d_b	bubble diameter (m)	NLMPC	nonlinear model predictive controllers
d_{b0}	initiate bubble diameter (m)	PBE	population balance equation
D_g	gas diffusion coefficient (m^2/s)	PID	proportional-integral-differential
DMC	dynamic matrix control	PDI	polydispersity index
d_p	particle diameter (m)	Q(r, j)	dead polymer molecule of length r produced at a site of type j
D_t	reactor diameter (m)	r	number of units in polymer chain
ETC	error trajectory controller	Re_{mf}	Reynolds number of particles at minimum fluidization condition
FBR	fluidized-bed reactor	R_i	instantaneous consumption rate of monomer (kmol/s)
F_{cat}	catalyst feed rate (kg/s)	R_p	production rate (kg/s)
FDM	fuzzy decision making	R_v	volumetric polymer outflow from the reactor (m^3/s)
f_i	fraction of total monomer in the reactant gas which is monomer M_i	SISO	Single-input-single-output
FIS	fuzzy inference system	T	temperature (K)
FH	fuzzy Hammerstein	t	time (s)
FLC	fuzzy logic controller	T_{in}	temperature of the inlet gaseous stream (K)
g	gravitational acceleration (m/s^2)	T_S	Takagi-Sugeno fuzzy inference system
GPC	gel permeation chromatography	T_{ref}	reference temperature (K)
H	height of the reactor (m)	U_t^*	dimensionless terminal falling velocity coefficient
H_2	hydrogen	U_0	superficial gas velocity (m/s)
H_{bc}	bubble to cloud heat transfer coefficient ($W/m^3·K$)	U_b	bubble velocity (m/s)
H_{be}	bubble to emulsion heat transfer coefficient ($W/m^3·K$)	U_{br}	bubble rise velocity (m/s)
H_{ce}	cloud to emulsion heat transfer coefficient ($W/m^3·K$)	U_{mf}	minimum fluidization velocity (m/s)
HDPE	high-density polyethylene	U_t	terminal velocity of falling particles (m/s)
ICA	induced condensing agent	V	reactor volume (m^3)
i	monomer type	V_p	volume of polymer phase in the reactor (m^3)
I_m	impurity such as carbon monoxide ($kmol/m^3$)	W_b	weight of solids in the bubble phase (kg)
J	active site type	W_e	weight of solids in the emulsion phase (kg)
K_b	elutriation constant in bubble phase ($kg.m^2/s$)	X(n,j)	nth moment of chain length distribution for dead polymer produced at a site of type j
K_{bc}	bubble to cloud mass transfer coefficient (1/s)	Y(n,j)	nth moment of chain length distribution for living polymer produced at a site of type j
K_{be}	bubble to emulsion mass transfer coefficient (1/s)	Z-N	Ziegler-Natta catalyst
K_{ce}	cloud to emulsion mass transfer coefficient (1/s)	**Greek letters**	

$k_{dI}(j)$	deactivation by impurities rate constant for a site of type j	ΔH_R	heat of reaction (J/kg)
$k_{ds}(j)$	spontaneous deactivation rate constant for a site of type j	δ	volume fraction of bubbles in the bed
K_e	elutriation constant in emulsion phase (kg·m2/s)	ε_b	void fraction of bubble for Geldart B particles
$k_f(j)$	formation rate constant for a site of type j	ε_e	void fraction of emulsion for Geldart B particles
$k_{fhi}(j)$	transfer rate constant for a site of type j with terminal monomer Mi reacting with hydrogen	ε_{mf}	void fraction of the bed at minimum fluidization
$k_{fmi}(j)$	transfer rate constant for a site of type j with terminal monomer Mi reacting with monomer Mk	μ	gas viscosity (Pa.S)
$k_{fri}(j)$	transfer rate constant for a site of type j with terminal monomer Mi reacting with AlEt3	ρ_g	gas density (kg/m^3)
$k_{fsi}(j)$	spontaneous transfer rate constant for a site of type j with terminal monomer Mi	ρ_{pol}	polymer density (kg/m^3)
k_g	gas thermal conductivity (W/m·K)	ϕ_s	sphericity for sphere particles
$k_{hi}(j)$	rate constant for reinitiating of a site of type j by monomer Mi	**Subscripts and superscripts**	
$k_{hr}(j)$	rate constant for reinitiating of a site of type j by cocatalyst	1	ethylene
$ki_i(j)$	rate constant for initiation of a site of type j by monomer Mi	2	1-butene
$kp_{ik}(j)$	propagation rate constant for a site of type j with terminal monomer Mi reacting with monomer Mk	b	bubble phase
kp_{Ti}	propagation rate constant (m3/kmol·s)	e	emulsion phase
LDMC	linear DMC	i	component type number
LDPE	low density polyethylene	j	active site type number
LLDPE	linear low-density polyethylene	mf	minimum fluidization
MFI	melt flow index (g/10min)	pol	polymer
$[M_i]$	concentration of component i in the reactor (kmol/m3)	ref	reference condition
$[M_i]_{in}$	concentration of component i in the inlet gaseous stream	T,TT	Pseudo kinetic rate constants
MIMO	Multi-input-multi-output		

INTRODUCTION

Union Carbide's process technology, known as "UNIPOL" to produce polyethylene (Figure 1) is characterized by moderate operating conditions (e.g. low pressure and temperature) and is less energy intensive than the traditional high-pressure process (2000-3000 atm). High purity ethylene and catalyst are continuously fed into the fluidized-bed reactor, where ethylene and co-monomers such as 1-butene or 1-hexene are polymerized together at a pressure of 20-30 atm with a narrow temperature range.[1]

FIGURE 1

A crucial aspect is the tight temperature control in gas phase polymerization reactors. The aim is to make sure that the reaction zone temperature stays higher than the

reactants' dew point, but under the polymer's melting point; this is to avoid melting and subsequent particle agglomeration.[2] Consequently, most of the commercial gas phase polyolefin fluidized bed reactors work in such a small temperature range of 248 to 400 K.[3] Even so, temperature excursions have to be prevented since they can cause some remarkable deviations in product properties and lead to low catalyst productivity.[4] Lacking temperature control, industrial polyolefin reactors have the tendency to be subjected to undesired situations such as unsteady states, or temperature trips toward undesirable high reaction zone temperature which is above the polymer softening point.[5–9] Also noteworthy is that the maximum polyethylene production rates take place when they work in the unstable steady states which surely need a proper controller to make stable steady states.

A vital polymer property that should be carefully controlled is the polymer MFI. Even though MFI is a quantity to measure polymer processability and its rheological behavior, it has been shown that MFI correlate with the final product properties and is one of the main variables to decide on the properties of a specific polymer grade. Two main standards are used to decide the polymer MFI by putting the polymer under a certain weight and temperature and measure the weight of melted polymer that passes an orifice with a certain size. ASTM D1238 and ISO 1133 are the standards used throughout the industry which differ on the testing specifications. For example, MFI of different linear low-density polyethylene (LLDPE) grades may range from 0.1 to 5 g/10min or even higher for special uses. LLDPEs with high MFIs may be used in producing geomembrane, high strength film, food and industrial packaging, and shopping bags while applications such as molded containers, chemical and water tanks and traffic cone need polymers with lower MFI. Although MFI was impossible to be measured on-line previously, recent modern technology with invention of new methods and instruments gave us the opportunity to control this vital polymer property online.[10]

Despite the non-linear attribute of the chemical processes, most of them are still regulated by the linear controllers aided by the plant models that are linearized.[11,12] The Arrhenius behavior of the rate constants is one of the main reasons behind the non-linearity in chemical reactors in terms of energetic transport phenomena, however, reaction kinetics and complex flow patterns also have effects on the nonlinearity of this process. Similarly, constrained manipulated variables possibly will give saturation non-linearity. During recent decades, non-linear controller designs were suggested to control specific highly non-linear systems where precise control was the important criterion. It is easy to design the input-output linearizing controllers, but they are restricted to minimum-phase systems since the zero dynamics of the process must be stable for the non-linear inversion.

Several researchers have studied controlling the main variables in olefin polymerization process using FBRs. McAuley and Macgregor[13] studied the non-linear model inverse-based control of polymer melt flow index (MFI) and density during grade changeover by manipulating hydrogen and butene feed concentration. They concluded that the nonlinear controller shows superior performance compared to a linear one and how essential it is to take nonlinearities into account for good product property control. Dadebo et al.[2] controlled the temperature and showed that the nonlinear error trajectory controller (ETC) shows better performance when compared to an optimally-tuned PID controller and showed that nonlinear controllers have an advantage as they are more capable in rejecting disturbances and ensure stability. Ali et al.[14] have tried to control monomer concentration and reactor temperature using improved single-input-single-output (SISO) and multi-input-multi-output (MIMO) PI-based controllers by manipulating the catalyst feed rate, U_0/U_{mf} ratio and feed temperature. Sato et al.[15] designed a model inverse optimal MIMO servo controller with integral actions plus an attached nonlinear compensator to control the MFI and polymer density by altering the fresh hydrogen and butene feed concentrations.

A number of researchers tackled this topic by employing nonlinear model predictive controllers (NLMPC). Hedengren et al.[16] used moving horizon estimation (MHE) to estimate new model parameters based on new plant data and have used the model for an NLMPC to control 26 control variables by altering 10 manipulated variables. In another work, Ali and Ali[17], used NLMPC to control polymer molecular weight distribution (MWD) by manipulating the ratio of monomer to hydrogen.

In relation to using intelligent controllers for gas-phase olefin polymerization in FBRs, one two works were found to utilize artificial intelligence (AI) or expert system-based controllers to maintain the system at optimal conditions and reject disturbances. Ghasem16 discussed that an effective way of handling nonlinearities present in this process is to use fuzzy logic. He recommended that because of the high accuracy in using PI controller at steady state and high performance of fuzzy logic in transient state, a grouping between the two can give an optimal solution. The author applied this hybrid controller in regulation of the reaction temperature by manipulating the cooling water inlet temperature to the heat exchanger. The results showed that the hybrid controller can significantly improve the severe oscillations that a sole fuzzy logic controller (FLC) produces. Ibrehem et al.[18] developed a model to take into account the presence of particles participating in the reaction with emulsion and catalyst phases and implemented a neural-network based predictive controller for controlling the temperature of the polyethylene system. He compared it with conventional controllers and showed that their neural network based adaptive controller gives better results in comparison with those PI controllers. Although polymer MFI is a very important polymer property, controlling it was not discussed in these two studies. Furthermore, using fuzzy logic alone needs an expert knowledge to define membership functions while neural networks provides a great tool to do this task for nonexpert designers. Benefiting from both these tools was the aim of designing the controller that is presented in this study.

In this study, a newly published dynamic two-phase ethylene copolymerization model[19] is used to simulate the process in order to study different control structures. This is a two-phase model which takes particle entrainment into account and the related equations are integrated with kinetic, hydrodynamic and transport phenomena equations. In the process control study, application of intelligent controllers on this highly nonlinear system is examined. For this objective, a SISO hybrid adaptive neuro-fuzzy inference system (ANFIS)-PID controller is used to both stabilize temperature at setpoints below the polyethylene's melting point and to reject temperature excursions resulting from disturbances. Furthermore, the ANFIS controller is used to control the polymer MFI with the aim of minimizing settling time and overshoot which are necessary for grade transition practices.

METHODOLOGY

A lot of research has been done on either mathematical modeling[20–22] or computer fluid dynamics (CFD) modeling[23–26] of this system. For testing the control structures, our newly modified dynamic model for ethylene copolymerization[19] is adopted. It is a two-phase and two-site copolymerization kinetic and hydrodynamic modeling structure for 1-butene and ethylene to help to get a further pragmatic view on heterogeneous ethylene copolymerization over Z-N catalyst in an FBR. Particle elutriation is embedded in the model to consider particle loss from the reactor bed which brings about a more improved model. This model helps to design and test new intelligent controllers that is discussed in this work.

Polymerization model

As established in the present work, the kinetic model suggested Abbasi et al.[19] produced an inclusive mechanism which details the 1-butene and ethylene copolymerization over Z-N catalyst. Parallel and series reactions in catalytic ethylene copolymerization with alpha-olefin

copolymers contribute to the complication of the process. The detailed multi-site kinetic model recommended weighs upon heterogeneous olefin copolymerization over Z-N catalysts. Important polymerization reactions as mentioned in their work can be referred to in Table 1. The most often used technique for polymerization modeling is the method of moments. The reason for this is that, by using this method, polymer properties and branching frequency, besides the means to estimate operational variables, can be foretold. These moment formulas are provided in Table 2 in which index i and j refer to the monomer and active site types respectively. Table 3 gives each reaction's rate constant for both site types and their literature sources.

TABLE 1

TABLE 2

TABLE 3

With the assumption that monomers are largely used during the propagation reactions, each component's rate of consumption can be obtained after solving the moment equations:[22]

$$R_k = \sum_{i}^{m} \sum_{j}^{ns} [M_k] Y(0, j) k_{p_{ik}} \quad (1)$$

Where m is the number of monomer and ns is the number of active site types. Subsequently, the overall polymer production rate can be attained:

$$R_p = \sum_{k=1}^{m} m w_k R_k \quad (2)$$

The polymerization is presumed to occur in both bubble and emulsion phases in this model. The equations required to compute the mass and heat transfer coefficients, velocities in the emulsion and bubble phases, and other valuable details in the copolymerization model are set down in Table 4. The list of assumptions made in the dynamic two-phase copolymerization model is given below:

- Polymerization reactions are presumed to happen in both bubble and emulsion phases.
- The emulsion phase is entirely mixed, and it does not stay at the minimum fluidization condition.
- The bubbles are constant size spheres and move with a velocity that stays unchanged over the bed at the plug flow condition.
- Temperature and concentration radial gradients in the reactor resulting from the rigidity of mixing resulting from the up-flowing gas are ignored.
- Entrainment of solids is considered at the uppermost segment of the bed.
- Heat and mass transfer resistance among solid particles and gas in the bubble and emulsion phases are not accounted for.
- Consistent particle size over the bed is taken into account.

Mass and energy balances that are formed considering these assumptions are given in Table 5. One does not fail to include the solid entrainment from the reactor topmost section since there are occasions in which the elutriation rate cannot be dismissed. In normal circumstances, a lot of the coarse particles stay in the reactor bed while the fluidizing gas makes the smaller ones to leave from the reactor. Nonetheless, when gas velocity becomes several times higher than the terminal velocity, particles with bigger size may be entrained from the bed as well.[27] This case is labeled particle entrainment or carry over and is highly crucial in both designing and operating of FBRs. Meanwhile, particle elutriation which is sometimes used interchangeably with particle entrainment which occurs in fact in the FBR cyclone that is placed outside the reactor in which the solids are moved apart from the fluidizing gas before returning to the reactor and after some processing. The implication is that in situations where the particle entrainment arises, their effect on the process must be deliberated. In effect, in the model used in this study, solid entrainment is considered to perform mass and energy balances to give more

realistic results when compared to the real data. The correlations for calculating the rate of solids entrainment are highlighted in

Table 6. Furthermore, MWD which is a significant polymer property is also included in the model to examine the model validity when it is compared to the industrial data.

TABLE 4

TABLE 5

TABLE 6

The following initial conditions are used to find the solution of these equations:

$$[M_i]_{b,t=0} = [M_i]_{in}$$
$$T_{b,t=0} = T_{in}$$
$$[M_i]_{e,t=0} = [M_i]_{in}$$
$$T_{e,t=0} = T_{in}$$

Molecular weight and Melt Flow Index (MFI) are polymer properties which are crucial for estimating the polymer quality, have been computed using the modified model used in this work.

The number averaged molecular weight is described as the mean of all the molecular weights of polymer sample's chains, defined by:

$$\bar{M}_n = \frac{\sum N_i M_i}{\sum N_i} \quad (3)$$

where N_i is the number of chains and M_i is the chain's molecular weight. $\bar{M}_n$ is quantified using methods that give the sum of molecules present in a weight's sample and can be estimated through various polymerization mechanisms. If $\bar{M}_n$ is stated for a specific MWD, this writes down that equal numbers of molecules exist on both sides of the M_n in the distribution. Conversely, the weight average molecular weight is defined by:

$$\bar{M}_w = \frac{\sum N_i M_i^2}{\sum N_i M_i} \quad (4)$$

Compared to $\bar{M}_n$, $\bar{M}_w$ takes a chain's molecular weight into account to figure out how it commits to the average molecular weight. If the chain gets bigger, the influence of chain on M_w would be greater. Weight average molecular weight, in lieu of the sum of molecules, is given by methods that quantify the molecular size e.g. light scattering techniques. If $\bar{M}_w$ is

stated for a specific MWD, this says that equal weight of molecules exists on both sides of M_w in the distribution.

The relationship between the molecular weight and MFI of polyethylene leans on the equation suggested by McAuley et al.[22], in which its constants are modified to be compatible with the real industrial data and is defined by:

$$MFI = 3.346 \times 10^{17} \bar{M}_W^{-3.472} \quad (5)$$

Advanced control strategies

For the control studies of MFI and temperature, the conventional PID controllers were first tested to see how they perform with this nonlinear system. The PID controllers were tuned using Ziegler-Nichols' closed loop method. Then, to overcome the limitations of the conventional methods, a neuro-fuzzy subclass of intelligent controllers, namely ANFIS controller, was used.

ANFIS is a type of artificial neural network that is constructed on Takagi–Sugeno fuzzy inference system[28]. The fuzzy logic approach is based on predefined rules (if-then) that does not have the ability to learn and adjust them to new conditions. Thus, to overcome this drawback, Jang[29] hybridized a fuzzy inference system (FIS) with an artificial neural network (ANN) to form ANFIS. The ANFIS methodology can be considered as an adaptive system in the form like ANN in which by training the system the parameters of the fuzzy membership functions (antecedent parameters) and the parameters of the fuzzy system output function (consequent parameters) are adapted[30]. ANFIS possesses the advantage of both FIS and ANN and it has solved the drawbacks of both systems, where the complicated procedures of neural networks are bypassed by applying linguistic variables of FIS system, and the weakness of FIS is solved by applying the neural inference system which create the ability to learn and adapt

itself to new condition. Further details about ANFIS is given in the attached Appendix: Adaptive Neuro-Fuzzy Inference System (ANFIS)

The Hybrid ANFIS-PID controller combines two controller types in one structure to receive help from individual capabilities of them to achieve one goal. The hybrid ANFIS-PID controller is based on a selecting or switching hybrid structure. In this structure, the controller action is divided into two regions. The output of PID controller is the main control signal and the output of ANFIS controller is the recovery control signal which is switched based on the value of three variables to determine the selecting hybrid controller which are the specified error threshold (ΔE_{error}), PID control signal (U_{PID}) and ANFIS control signal (U_{ANFIS}). The error threshold is defined based on the requirements of the studied system. The block diagram and decision-making flowchart of hybrid PID-ANFIS controller is shown in Figure 2.

$$U_{hybrid} = \begin{cases} U_{PID}, & \text{for } Error < \Delta E_{error} \\ U_{ANFIS}, & \text{for } Error \geq \Delta E_{error} \end{cases} \quad (6)$$

FIGURE 2

Figure 3 and Figure 4 show the type and values of membership functions for inputs of the designed MFI and temperature ANFIS controllers respectively.

FIGURE 3

FIGURE 4

Table 7 shows the specifications of the designed ANFIS controllers for controlling both MFI and temperature.

TABLE 7

Modeling and simulation of the proposed model and control scheme was done using MATLAB® and Simulink® suit. The model of the process was written in MATLAB® and was linked to Simulink® as a process block with several inputs and outputs. The dynamic equations are solved using a variable step numerical solver given the inputs to produce the outputs. This

makes it possible to design and test controller to control desired outputs by manipulating the block inputs. Each simulation takes almost 2 to 10 seconds using a normal desktop computer utilizing an Intel® Core™ i7-6700HQ processor.

RESULTS AND DISCUSSION

The validation of the model proves to be crucial. This was carried out using industrial data[19] that include the production rate, MWD and transient reactor temperatures. The results rest on the BP LL0209 grade polyethylene operating conditions which is a licensed linear low-density polyethylene.

Polymer production rate of the FBR versus residence time is illustrated in Figure 5. This figure demonstrates the production rate evolution from when the Ziegler-Natta catalyst goes into the reactor and the reaction begins up until the bed fully fluidizes and the production becomes steady. This figure as well highlights the production rate evolution of the polymer in both the emulsion and bubble phases over time in the reactor. The computed total value ascends from nearly 7 tons to almost 10 tons within the first and second hours of operation and turn steady after nearly 5 hours of production at 13.44 tons. To demonstrate that the model is right while confirming the results, the polymer production rate was drawn versus the actual industrial data. The horizontal line that shows the actual steady state data is the production rate value in the industrial FBR. As can be seen, the steady state value of production rate was predicted accurately enough by the model with only 0.4 ton deviation. To illustrate the effect of taking particle elutriation into account, the results of another work from literature[31] that do not consider this fact is given in this figure. When particles leave the column, less catalyst exist in the reactor resulting in lower reactions and less production rate. The figure also shows that almost 60 percent of the polyethylene is made in the emulsion phase and nearly 40 percent of the overall production occur inside the bubble phase.

FIGURE 5

Additionally, the computed stable state MWD was compared with industrial MWD data points in Figure 6. The actual data was produced through gel permeation chromatography. In this figure, the calculated cumulative weight fraction derivative is plotted versus the logarithm of weight average molecular weight, where it is a characteristic gel permeation chromatography (GPC) result. Notably, other than the very slight differences, these sets of data have shown a great consistency.

FIGURE 6

To add, the industrial data was plotted versus the estimated reactor temperatures in Figure 7. The model was found to have the potential to accurately estimate the temperature of the reactor for this polymer grade. The mean 0.6 percent difference from the industrial data is acceptable and small in the engineering context. That said, by giving some weight on the heat transfer resistance among solid particles and gas in both phases, particle size distributions and radial temperature gradients in the reactor, the model can be improved further, leading to better polymer properties and reactor parameters predictions. Nevertheless, the model intricacy and computational labors will be increased.

FIGURE 7

MFI control

The modified two-phase model[19] as has been discussed earlier, is employed for the control studies since it has been validated with the actual process. To show the non-linear performance of the ethylene copolymerization FBR, the model underwent a simulation for step changes in the inlet hydrogen concentration, as the process key parameter to affect the polymer MFI. The open-loop simulation results can be referred to in Figure 8.

In Figure 8, the inlet hydrogen concentration was altered after the reactor reached the steady state. The inlet hydrogen concentration has a considerable impact on the polymer MFI. In this case, inlet hydrogen concentration experience incremental step changes from 2 percent to 18 percent of hydrogen with 2 percent increase in each of the open-loop runs. This figure indicates that the hydrogen concentration in the feed has considerable effects on the MFI and non-symmetric responses are yielded. This means that the polymer MFI variates with the changes in inlet hydrogen concentration nonlinearly. When talking about the nonlinear behavior, implementation of conventional controllers results in deficient control of the process variables. This clarifies using a better suited advanced control system to adjust the impact of hydrogen concentration on the desired variables within the process. This justifies the implementation of a more effective advanced control system to appropriately control the hydrogen concentration effect on the process variable. Moreover, Figure 8 also shows that MFI has inherently very slow dynamics and it takes 5-10 hours to reach steady state after a step change in the open loop configuration.

FIGURE 8

MFI control- setpoint tracking

Figure 9 shows the MFI set point changes between 1 and 1.4 g/10min tracked by PID and ANFIS controllers with 0 to 20 percent saturation values respectively. This figure illustrates that both controllers are capable of set-point tracking. Even though the PID controller reaches the set-point in every step change after a while, the ANFIS controller performance outperforms the PID controller as it has very small overshoots and has much less response times. For example, during the second step change from 1.4 to 1.3 g/10min at 2×10^5 seconds, it takes the PID controller around 3 hours to settle but it takes only 13 minutes for the ANFIS controller to settle with a negligible post-transition undershoot of 0.015 g/10min in the MFI value.

FIGURE 9

The controller moves of ANFIS and PID controllers in MFI set point tracking are further shown in Figure 10. The controllers are constrained to a maximum 20 percent of hydrogen inlet concentration to make polymerization workable and realistic. To illustrate, it is found that the starting point of hydrogen concentration must be 9.6 percent to set the MFI at 1 g/10min. However, after a step change to 1.4 g/10min, the controllers should set the inlet concentration to 11.5 percent. The controller moves of the ANFIS controller is fast and realistic. It fluctuates two times from minimum to the maximum of the manipulated variable and then some oscillations before reaching a steady state and this takes around 25 minutes for the ANFIS controller. On the other hand, PID controller jumps to the maximum and suddenly to the minimum of the manipulated variable before starting to rise slowly to reach the right value after a prolonged period of almost 8 hours. This shows that the ANFIS controller was much faster and robust in following the MFI setpoint, while the PID moves were more extreme and drastic in its controller moves.

FIGURE 10

MFI control-disturbance rejection

To verify that a controller can be employed in the industrial trials, it must be prepared to handle regulatory complications successfully as well. In the case of MFI, as Figure 11 shows, the concentration of ethylene has nonlinear and non-proportional effects on the MFI value such that increasing ethylene concentration in the feed leads to polymers with higher density and lower MFI which may get above or below allowable specifications. As a result, variation in ethylene concentration was used as disturbance to test predictability and robustness of these controllers.

FIGURE 11

Figure 12 displays the MFI response when it is controlled by ANFIS and PID controllers with a disturbance of 50 percent deduction in inlet ethylene concentration after 1.5×10^5 seconds. This figure shows clearly that the ANFIS controller is capable of disturbance rejection in a faster and more effective manner as compared to the PID controller.

FIGURE 12

As shown, since MFI has slow dynamics, ANFIS controller can completely omit the effect of the disturbance by rapidly changing the manipulated variable within just 8 minutes (Figure 13). However, although the disturbance makes little deviation from the set point in case of the PID controller, it takes almost 19 hours for it to retract the system to the stable set-point. This is due to the less sensitiveness of the PID controller in this case with very slow decrease that it makes in the manipulated variable for compensating the disturbance effect.

FIGURE 13

The measures of controlled system performance in terms of the integral of time absolute error (ITAE), the integral of absolute error (IAE), integral of squared error (ISE), and absolute percentage error (APE) for each MFI controller in both disturbance rejection and set-point tracking cases was also computed and is listed in Table 8. It is shown by the error values that the ANFIS controller showed improved performance compared to PID since all the performance index values for the ANFIS controller is lower than the PID controller in both the disturbance rejection and set-point tracking studies.

TABLE 8

Temperature control

Characteristically, the ethylene copolymerization reaction is very much exothermic. To keep the polyethylene production rates at the preferable values, it is important to make sure that the reactor's temperature is higher than reactants' dew point to prevent gas condensation within

the reactor. Retaining the temperature below the polymer melting point is also necessary so that the particle melting, and agglomeration can be prevented, or the reactor will shut down. Consequently, an effective temperature control system must be implemented.

In this study, cooling water flow rate in terms of its valve opening percentage to the recycle stream heat exchanger is used as the manipulated variable of the controller. Figure 14 shows how the reactor temperature changes with incremental changes in valve opening for the cooling water flow rate. Exothermic reaction takes place in this reactor, therefore, reducing the cool water flow rate of the recycle stream heat exchanger leads to higher temperatures in the reactor.

FIGURE 14

Figure 15 illustrates how fully closing and opening the cool water valve impacts the reactor temperature. As seen, unlike the case of MFI, here we have faster and responsive dynamics. While it took nearly 10 hours for the MFI to reach steady state after changing the manipulated variable from 10 percent to 20 percent, it takes the temperature only 2.5 hours to get to the steady value after altering the manipulated variable from 0 percent to 100 percent and vice versa. This shows the response dynamics are different in this case and we may need an advanced controller design here.

FIGURE 15

Temperature control – setpoint tracking

Temperature control design also needs to be tested with step changes in set point and see how the controller follows it. Firstly, a conventional PID controller with 0 to 100 saturation values was tuned using the Ziegler-Nichols' closed loop method and tested in the servo scenario which is shown in Figure 16. As illustrated, rising, or falling time is short (200-400 seconds) and the controller eventually reaches and follows the setpoint. However, there is overshoots in both

kinds of step changes where the duration and peak of it depends on the increase or decrease percentage in the setpoint. For increasing cases, it takes around 2.5 hours with a peak of almost 2 K overshoot in temperature while decreasing the setpoint leads to some oscillation with around ±1 K overshoot and undershoots and with settling times of nearly half an hour.

The difference in temperature response to raising or lowering of the set points has a reason. In the case of a temperature increase the only thing that controller can do is to fully close the cool water valve and let temperature rise in the system because of the exothermic reaction. On the other hand, to decrease the temperature, controller fully opens the valve. Since rising time for temperature increase is higher than falling time for temperature decrease, system gets cool faster than it gets hot in this system and with this specific heat exchanger capacity.

In this nonlinear system case, the only problem with the PID controller is the overshoots and undershoots. To alleviate this issue, we need to think of other advanced controllers which can control the process efficiently.

FIGURE 16

An ANFIS controller was designed and trained for controlling the temperature by manipulating the cool water valve and the result is presented in Figure 17. The ANFIS controller improves the performance of the PID controller disadvantages but shows some oscillations around the setpoint. Depending on the amount of step change, these oscillations are within ± 0.2 K of the setpoint with periods of around 5 minutes. This effect is because of the fast dynamics of the system and fuzzy rule changes of the ANFIS controller.

FIGURE 17

To mitigate the problems with both controllers, both controllers were used to control the temperature in a hybrid design and the result is illustrated in Figure 18. The main controller of this hybrid controller structure is the ANFIS controller and when the PID controller has passed its overshoot period, the controller switches to the PID to stick to the setpoint with no

oscillations. This is made possible by setting a switching threshold of 0.2 degrees of error meaning the controller switches to the PID controller only after its error is less than this value.

FIGURE 18

Figure 19 shows the control moves for all three types of the temperature controllers. As can be seen, hybrid controller was again superior in performance since it greatly reduced the oscillations. The cold-water valve opening and closing gradually takes place almost every 3 minutes within the oscillatory range which is acceptable for a control valve.

FIGURE 19

Temperature control – disturbance rejection

Several different step changes in the velocity of superficial gas was applied on the model to examine possible disturbances on the reactor temperature, as a key process parameter. The open-loop simulation result is shown in Figure 20. In this figure, after the reactor continues to work in steady state for a while, superficial gas velocity was altered with both additive and deductive increments which led to non-symmetrical responses. This figure suggests that superficial gas velocity has a significant effect on the reactor temperature. Furthermore, positive steps in the superficial gas velocity have less effects on the reactor temperature in comparison with the matching negative steps. To put simply, the reactor temperature changes in a non-linear manner with the superficial gas velocity. With the demonstration of the nonlinear behavior, the conventional controllers lead to the process variables being poorly controlled. This justifies clearly the need to implement a more effective control system to control the superficial gas velocity effect on the process variable efficiently.

FIGURE 20

To examine the system response to superficial gas velocity disturbance, a high reduction of 50 percent in the process variable is introduced at 5×10^4 seconds. The controller responses are

given in Figure 21. Once again, PID was unable to mitigate the disturbance and responded with an overshoot and a settling time of almost 3 hours. ANFIS controller starts to gradually diverge the oscillations from the set point with increase in the periods of oscillations. On the other hand, hybrid controller has successfully absorbed the effect of the disturbance and performed like a step change case where the ANFIS controller takes over right after the change and switches to PID afterwards.

FIGURE 21

Controller moves of temperature controllers are given in Figure 22. The same trend of control variable is seen here again. PID takes a lot of time to find the correct value, ANFIS starts to destabilize after the disturbance point and hybrid controller behave as before.

FIGURE 22

Table 9 lists the calculated measures of the controlled system performance for different temperature controller designs in both disturbance rejection and set-point tracking scenarios. The info shows the superiority of the hybrid controller in terms of performance compared to both PID and ANFIS alone since the ITAE, IAE, ISE and APE values for the hybrid controller prove to be the smallest in both disturbance rejection and set-point tracking studies.

TABLE 9

CONCLUSIONS

A dynamic two-phase ethylene copolymerization model was taken up to describe the dynamics in FBRs. The particle entrainment from the FBR is considered by the model. The hydrodynamics is integrated with a kinetics of copolymerization (ethylene and 1-butene) to give an improved knowledge of the reactor performance. The modified dynamic two-phase ethylene copolymerization model performance resembled the actual industrial conditions to a great deal, where the temperature foretold by the model was close to the real plant data. The

model was then adopted to perform further control examinations. A right choice of controllers that can be used by industries were implemented to address both the servo and regulatory control of the polymer MFI as a fundamental polymer property and reactor temperature as a very crucial process parameter. The simulation results showed that reactor temperature can be controlled by altering the cold-water flow rate and MFI by changing the hydrogen concentration in the feed. Conventional controllers showed that they perform poorly compared to the intelligent controllers due to their linear nature. For instance, PID controller takes around 2.5 hours to settle with 2K overshoot when the temperature setpoint changes from 343K to 350K while it takes around 30 minutes for the hybrid ANFIS-PID temperature controller to settle with only 0.2K overshoot. ANFIS-based controllers showed to be promising as they have faster settling times and less overshoots in both servo and regulatory control situations. This work can be extended in future by adding ANFIS-based MIMO controllers which makes it possible to simultaneously control several variables using one main controller. Other control variables that can be considered are polymer density, MWD, polydispersity index and production rate. Another interesting work would be to dynamically optimize the controller and model parameters online on a pilot plant using its transitory measured data.

ACKNOWLEDGMENTS

The authors would like to thank the support of the Ministry of Higher Education Malaysia (MOHE) through research grant (FP064-2015A) and Postgraduate Research Grant (PPP) project No. PG131-2014A.

REFERENCES

1 Atan FM, Hussain AM, Abbasi RM, Khan JM, and Fazly Abdul Patah M, Advances in Mathematical Modeling of Gas-Phase Olefin Polymerization. *Processes* **7** (2019).

1 2 Dadebo SA, Bell ML, McLellan PJ, and McAuley KB, Temperature control of industrial gas phase polyethylene reactors. *J Process Control* **7**:83–95 (1997).

3 3 Xie T, McAuley KB, Hsu JCC, and Bacon DW, Gas Phase Ethylene Polymerization: Production Processes, Polymer Properties, and Reactor Modeling. *Ind Eng Chem Res* **33**:449–479 (1994).

6 4 Shamiri A, Wei S, Fauzi M, Hussain MA, and Mostoufi N, Modified two-phase model with hybrid control for gas phase propylene copolymerization in fluidized bed reactors. *Chem Eng J* **264**:706–719.Elsevier B.V. (2015).

9 5 McAuley KB, Macdonald DA, and McLellan PJ, Effects of operating conditions on stability of gas-phase polyethylene reactors. *AIChE J* **41**:868–879 (1995).

11 6 Choi K-Y and Harmon Ray W, The dynamic behaviour of fluidized bed reactors for solid catalysed gas phase olefin polymerization. *Chem Eng Sci* **40**:2261–2279 (1985).

13 7 Ghasem NM, Effect of Polymer Particle Size and Inlet Gas Temperature on Industrial Fluidized Bed Polyethylene Reactors. *Chem Eng Technol* **22**:777 (1999).

15 8 Ho YK, Shamiri A, Mjalli FS, and Hussain MA, Control of industrial gas phase propylene polymerization in fluidized bed reactors. *J Process Control* **22**:947–958 (2012).

18 9 Shamiri A, Hussain MA, Mjalli F sabri, Mostoufi N, and Hajimolana S, Dynamics and Predictive Control of Gas Phase Propylene Polymerization in Fluidized Bed Reactors. *Chinese J Chem Eng* **21**:1015–1029 (2013).

21 10 Abbasi MR, Shamiri A, and Hussain MA, A review on modeling and control of olefin polymerization in fluidized-bed reactors. *Rev Chem Eng* (2018).

23 11 Hisbullah, M. H, and K. R, Comparative evaluation of various control schemes for fed-batch fermentation. *Bioprocess Biosyst Eng* **24**:309–318 (2002).

25 12 Mjalli FS, Kim San L, Chai Yin K, and Azlan Hussain M, Dynamics and Control of a

Biodiesel Transesterification Reactor. *Chem Eng Technol* **32**:13–26.WILEY-VCH Verlag (2009).

13 McAuley KB and Macgregor JF, Nonlinear product property control in industrial gas-phase polyethylene reactors. *AIChE J* **39**:855–866 (1993).

14 Ali EM and Abasaeed AE, Improved Regulatory Control of Industrial Gas-Phase Ethylene Polymerization Reactors. *Ind Eng Chem Res* **38**:2383–2390 (1999).

15 Sato C, Ohtani T, and Nishitani H, Modeling, simulation and nonlinear control of a gas-phase polymerization process. *Comput Chem Eng* **24**:945–951 (2000).

16 Hedengren JD, Allsford K V, and Ramlal J, Moving Horizon Estimation and Control for an Industrial Gas Phase Polymerization Reactor, *2007 Am Control Conf*, 1353–1358, New York, NY (2007).

17 Al-haj Ali M and Ali EM, Effect of monomer feed and production rate on the control of molecular weight distribution of polyethylene in gas phase reactors. *Comput Chem Eng* **35**:2480–2490 (2011).

18 Ibrehem AS, Hussain MA, and Ghasem NM, Mathematical Model and Advanced Control for Gas-phase Olefin Polymerization in Fluidized-bed Catalytic Reactors. *Chinese J Chem Eng* **16**:84–89 (2008).

19 Abbasi MR, Shamiri A, and Hussain MA, Dynamic modeling and Molecular Weight Distribution of ethylene copolymerization in an industrial gas-phase Fluidized-Bed Reactor. *Adv Powder Technol* **27**:1526–1538 (2016).

20 Kiashemshaki A, Mostoufi N, Sotudeh-Gharebagh R, and Pourmahdian S, Reactor Modeling of Gas-Phase Polymerization of Ethylene. *Chem Eng Technol* **27**:1227–1232 (2004).

21 Alizadeh M, Mostoufi N, Pourmahdian S, and Sotudeh-Gharebagh R, Modeling of fluidized bed reactor of ethylene polymerization. *Chem Eng J* **97**:27–35 (2004).

22 McAuley KB, MacGregor JF, and Hamielec AE, A kinetic model for industrial gas-phase ethylene copolymerization. *AIChE J* **36**:837–850.American Institute of Chemical Engineers (1990).

23 Akbari V, Nejad Ghaffar Borhani T, Shamiri A, and Kamaruddin Abd. Hamid M, A CFD–PBM coupled model of hydrodynamics and mixing/segregation in an industrial gas-phase polymerization reactor. *Chem Eng Res Des* **96**:103–120.Institution of Chemical Engineers (2015).

24 Akbari V, Borhani TNG, Godini HR, and Hamid MKA, Model-based analysis of the impact of the distributor on the hydrodynamic performance of industrial polydisperse gas phase fluidized bed polymerization reactors. *Powder Technol* **267**:398–411.Elsevier B.V. (2014).

25 Karimi S, Mansourpour Z, Mostoufi N, and Sotudeh-Gharebagh R, CFD-DEM Study of Temperature and Concentration Distribution in a Polyethylene Fluidized Bed Reactor. *Part Sci Technol* **29**:163–178 (2011).

26 Li J, Luo Z-H, Lan X-Y, Xu C-M, and Gao J-S, Numerical simulation of the turbulent gas–solid flow and reaction in a polydisperse FCC riser reactor. *Powder Technol* **237**:569–580.Elsevier B.V. (2013).

27 Rhodes M, Introduction to Particle Technology, John Wiley & Sons Ltd, West Sussex (2008).

28 Burns RS, Advanced Control Engineering, Butterworth-Heinemann (2001).

29 Jang J-SR, ANFIS: adaptive-network-based fuzzy inference system. *IEEE Trans Syst Man Cybern* **23**:665–685 (1993).

30 Khosropanah P, Ramli AR, Abbasi MR, Marhaban MH, and Ahmedov A, A hybrid unsupervised approach toward EEG epileptic spikes detection. *Neural Comput Appl*:1–12 (2018).

31 Kiashemshaki A, Mostoufi N, and Sotudeh-Gharebagh R, Two-phase modeling of a gas phase polyethylene fluidized bed reactor. *Chem Eng Sci* **61**:3997–4006 (2006).

32 Lucas A, Arnaldos J, Casal J, and Puigjaner L, Improved equation for the calculation of minimum fluidization velocity. *Ind Eng Chem Process Des Dev* **25**:426–429.American Chemical Society (1986).

33 Kunii D and Levenspiel O, Fluidization Engineering, Butterworth-Heinemann (1991).

34 Mostoufi N, Cui H, and Chaouki J, A Comparison of Two- and Single-Phase Models for Fluidized-Bed Reactors. *Ind Eng Chem Res* **40**:5526–5532 (2001).

35 Hillegardt K and Werther J, Local bubble gas hold-up and expansion of gas/solid fluidized beds. *Ger Chem Eng* **9**:215–221.VCH (1986).

36 Cui H, Mostoufi N, and Chaouki J, Characterization of dynamic gas–solid distribution in fluidized beds. *Chem Eng J* **79**:133–143 (2000).

37 Shamiri A, Azlan Hussain M, Sabri Mjalli F, Mostoufi N, and Saleh Shafeeyan M, Dynamic modeling of gas phase propylene homopolymerization in fluidized bed reactors. *Chem Eng Sci* **66**:1189–1199 (2011).

38 Geldart D, Cullinan J, Georghiadas S, Gilvray D, and Pope DJ, The Effect of Fines of the Entrainment from Gas Fluidized Beds. *Trans Inst Chem Eng* **57**:269–275 (1979).

39 Haider A and Levenspiel O, Drag coefficient and terminal velocity of spherical and nonspherical particles. *Powder Technol* **58**:63–70.Elsevier (1989).

APPENDIX: ADAPTIVE NEURO-FUZZY INFERENCE SYSTEM (ANFIS)

ANFIS was developed as an adaptive system with a set of fuzzy rules (if-then) and tunable MF (membership function) parameters in a training phase. During the training phase of ANFIS, two different parameters should be perfected to give the learning procedures:

- antecedent parameters (the MF parameters)
- consequent parameters (the fuzzy system output function)

As the consequent parameters are linear, to optimize these parameters the linear least-squares method is applied and to optimize the antecedent parameters the back-propagation algorithm in conjunction with an optimization method such as the gradient descent is applied.

Five different layers construct the ANFIS structure while each layer consists of node functions and the inputs of the nodes in the present layer are obtained from earlier layers. The consecutive layers of ANFIS structure are as follows: layer 1 is fuzzification (if-part), layer 2 is production part, layer 3 is normalization part, layer 4 is defuzzification (then-part), and eventually layer 5 is total output generation part. Figure A1 shows the structure of ANFIS with two independent variables (x and y) as input and one dependent variable f_{out} as an output.

FIGURE A1

For fuzzy inference systems, difference in the consequence of the set of fuzzy rules (if-then) and defuzzification procedures lead to two distinct types of fuzzy inference systems known as Mamdani type FIS and Sugeno type FIS.

The main difference between Sugeno type FIS and Mamdani type FIS is the way the fuzzy inputs are converted to the crisp output. In Mamdani type FIS for computing the crisp output the defuzzification technique of a fuzzy output is used while in Sugeno type FIS the weighted average method is used. As the consequents of the rules are not fuzzy in the Sugeno

method, the interpretability and expressive power of Mamdani output, are eliminated in this method. In comparison to Mamdani type FIS, Sugeno has faster processing time since instead of the time consuming defuzzification process, the weighted average method is applied.

Moreover, another difference between Sugeno and Mamdani type FIS is that Sugeno has no output membership functions while Mamdani FIS has output membership so, Sugeno method gives an output that is either linear (weighted) mathematical expression or a constant. Instead, Mamdani method gives an output that is a fuzzy set. In comparison to Mamdani type FIS, Sugeno has more flexibility in system design as latter can be integrated with ANFIS tool to model the systems more precisely. Considering ANFIS with Sugeno type FIS, so the rule base of ANFIS holds fuzzy IF-THEN rules of a first order Sugeno type FIS are told as:

- Rule 1: If x is A_1 and y is B_1then z is $f_1(x, y; p_1, q_1, r_1) = xp_1 + yq_1 + r_1$
- Rule 2: If x is A_2 and y is B_2 then z is $f_2(x, y; p_2, q_2, r_2) = xp_2 + yq_2 + r_2$

where $f_i(x, y; p_i, q_i, r_i)$ is a first order polynomial function which stands for the outputs of the Sugeno type FIS, A_i and B_i are the fuzzy sets, and x and y are two different input and z is an output of ANFIS model.

In the ANFIS structure, different layers consist of different node function. As shown in Figure A1, adaptive nodes which stand for the adjustable parameter sets are denoted by squares while fixed nodes which stand for the fixed parameter sets in the system are denoted by circles.

***Layer 1*:** Every node in this layer is an adaptive node with a node function as follows:

$$Q_{1,i} = \mu_{A_i}(x) \quad i = 1,2 \tag{A.1}$$

$$Q_{1,i} = \mu_{B_i}(y) \quad i = 3,4 \tag{A.2}$$

Where x and y are the inputs to node i , $_i$ and B_i are linguistic labels, μ_{A_i} and μ_{B_i} are the membership functions for A_i and B_i fuzzy sets, respectively and $Q_{1,i}$ is the membership grade of a fuzzy set and considered as the output of node i in the first layer which specifies the degree to the given input (x or y) satisfies the quantifies.

Typically, in ANFIS, the MF (membership function) for a fuzzy set can be any parameterized membership function, such as generalized bell-shaped function, Gaussian, trapezoidal or triangular.

A generalized Bell-shaped MF (bell MF) is specified as follows:

$$\mu_A(x;a,b,c) = \frac{1}{1+\left[\frac{x-c}{a}\right]^{2b}} \tag{A.3}$$

A Gaussian MF is specified as follows:

$$\mu_A(x;;c,\sigma) = e^{-0.5\left(\frac{x-c}{\sigma}\right)^2} \tag{A.4}$$

while σ and c decide the width and center of Gaussian MF, respectively.

A trapezoidal MF is specified as follows:

$$\mu_A(x;;a,b,c,d) = max(min\left(\frac{x-a}{b-a},1,\frac{d-x}{d-c}\right),0) \tag{A.5}$$

The parameters with $a < b \leq c < d$ specify the x coordinates of the four corners for the underlying trapezoidal MF.

A triangular MF is specified as follows:

$$\mu_A(x;;a,b,c) = max(min\left(\frac{x-a}{b-a},\frac{c-x}{c-b}\right),0) \tag{A.6}$$

The parameters with $a < b < c$ specify the x coordinates of the three corners for the underlying triangular MF.

In this layer, the parameters a,b,c,d and σ are the antecedent parameters.

Layer 2: Every node in this layer is a fixed node whose output is the product of all the incoming signals. In this layer through multiplication of input signals the firing strength of each rule is figured out.

$$Q_{2,i} = w_i = \mu_{A_i}(x)\,\mu_{B_i}(y) \quad i = 1,2 \tag{A.7}$$

where w_i is output signal, which stands for the firing strength of a rule.

Layer 3: Every node in this layer is a fixed node. In this layer, the firing strength provided in earlier layer is normalized by computing the ratio of the i^{th} rule's firing strength to the sum of all rules' firing strengths.

$$Q_{3,i} = \overline{w}_i = \frac{w_i}{w_1 + w_2} \quad i = 1,2 \tag{A.8}$$

where $\overline{w}$ is output signal, which is the normalized firing strength of a rule.

Layer 4: In this layer every node i is adaptive with a node function.

$$Q_{4,i} = \overline{w}_i f_i \quad i = 1,2 \tag{A.9}$$

where f_1 and f_2 are the fuzzy IF-THEN rules as follows:

- Rule 1: If x is A_1 and y is B_1then z is $f_1(x, y; p_1, q_1, r_1)$
- Rule 2: If x is A_2 and y is B_2 then z is $f_2(x, y; p_2, q_2, r_2)$

Where $r_i q_i$, and p_i are the parameter set, referred to as the linear consequent parameters.

Layer 5: This layer has only one fixed node that computes the overall output of ANFIS by summation of all incoming signals as:

$$Q_{5,i} = f_{out} = \sum_i \overline{w}_i f_i = \frac{\sum_i w_i f_i}{\sum_i w_i} = overal\ output \quad i = 1,2 \tag{A.10}$$

The overall output is linear combination of the consequent parameters. Thus, the final output of ANFIS is expressed as

$$
\begin{aligned}
f_{out} &= \overline{w}_1 f_1 + \overline{w}_2 f_2 \\
&= \frac{w_1}{w_1 + w_2} f_1 + \frac{w_2}{w_1 + w_2} f_2 \\
&= \left(\overline{w}_1 x\right) p_1 + \left(\overline{w}_2 x\right) p_2 + \left(\overline{w}_1 y\right) q_1 + \left(\overline{w}_2 y\right) q_2 + \left(\overline{w}_1\right) r_1 + \left(\overline{w}_2\right) r_2
\end{aligned}
\tag{A.11}
$$

Eventually, ANFIS applies a hybrid learning algorithm for parameter tuning. It uses the back-propagation algorithm and the least squared method for updating the input MF parameters (antecedent parameters) in layer 1, and training the consequent parameters, respectively.

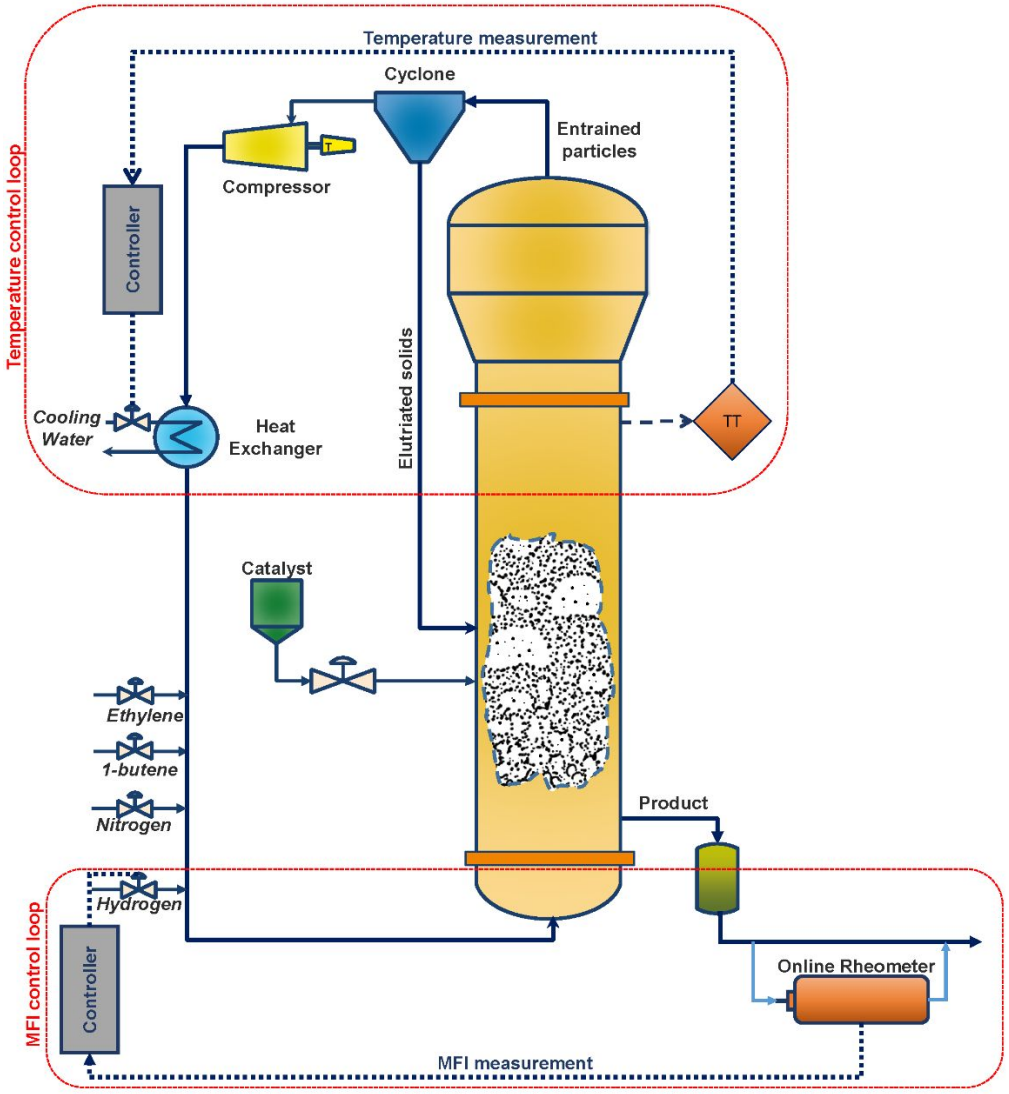

Figure 1: A typical fluidized bed polymerization reactor with temperature and MFI control loop structures.

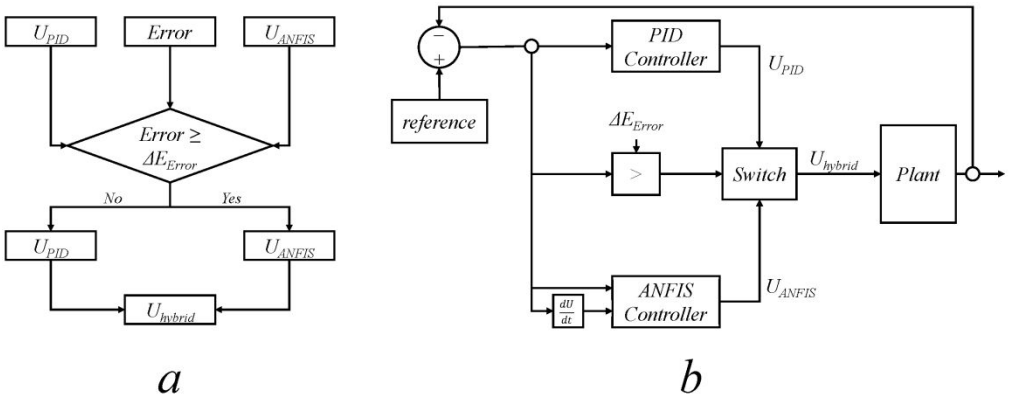

Figure 2: a) flowchart and b) block diagram of selecting hybrid PID–ANFIS controller

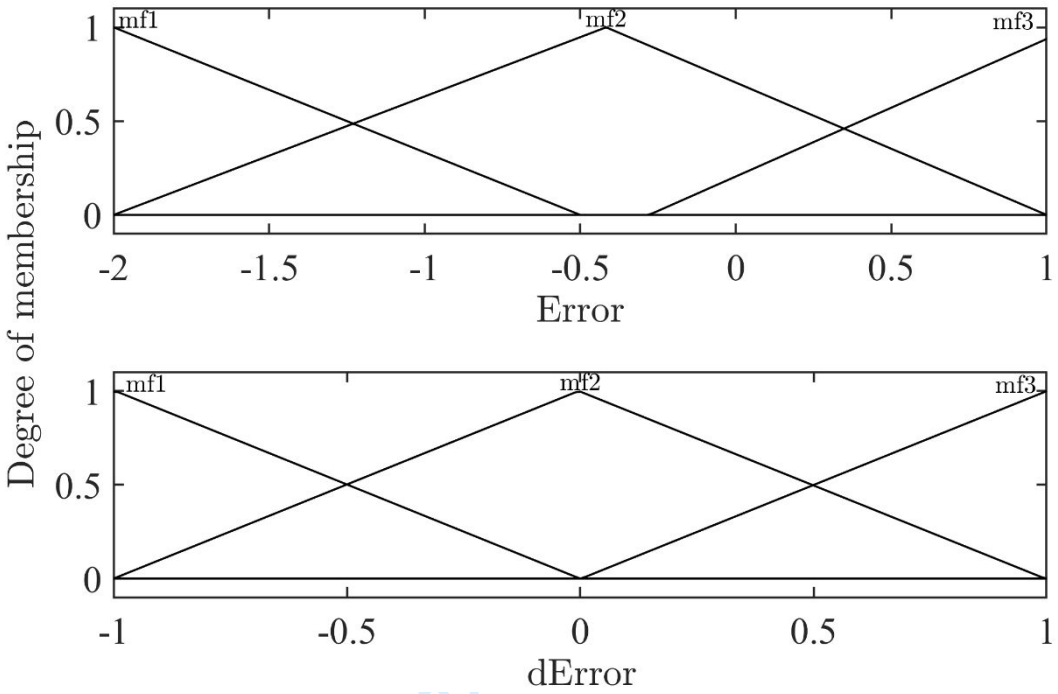

Figure 3: Input membership functions of the MFI ANFIS controller

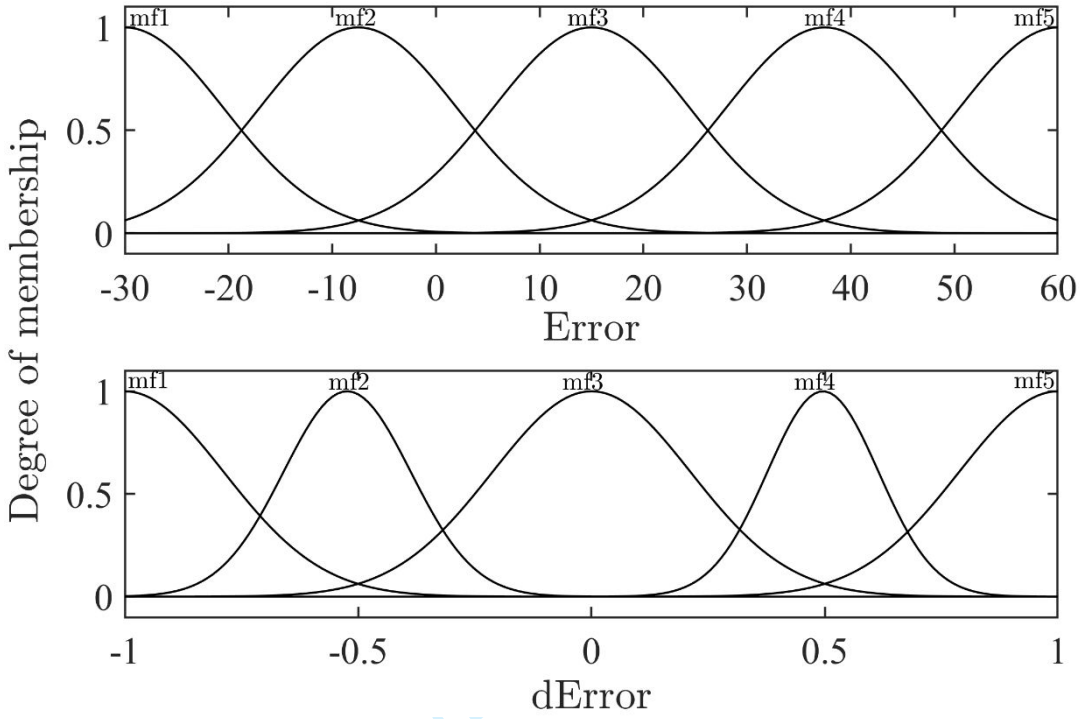

Figure 4: Input membership functions of the temperature ANFIS controller

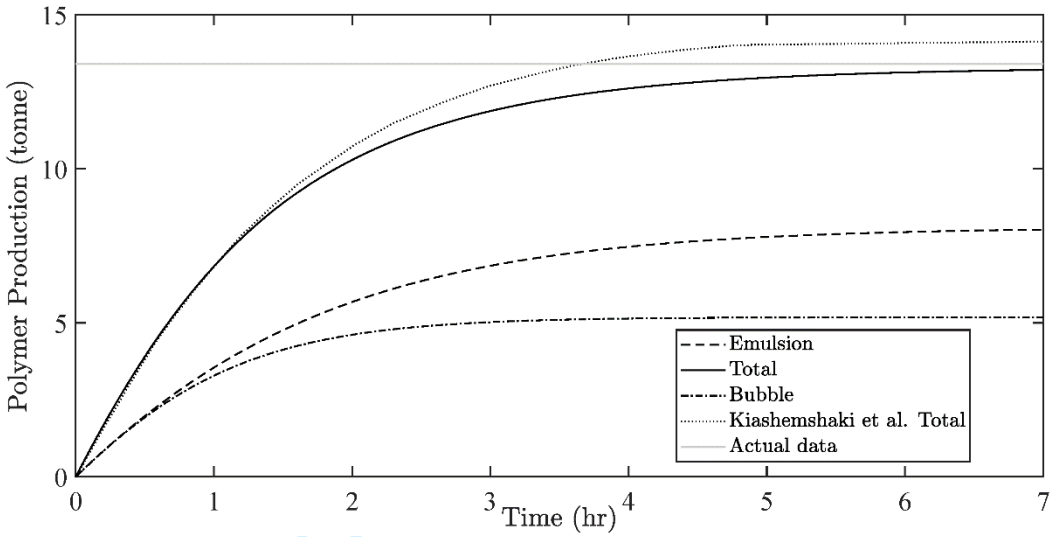

Figure 5: Polymer production rate evolution over time in the FBR

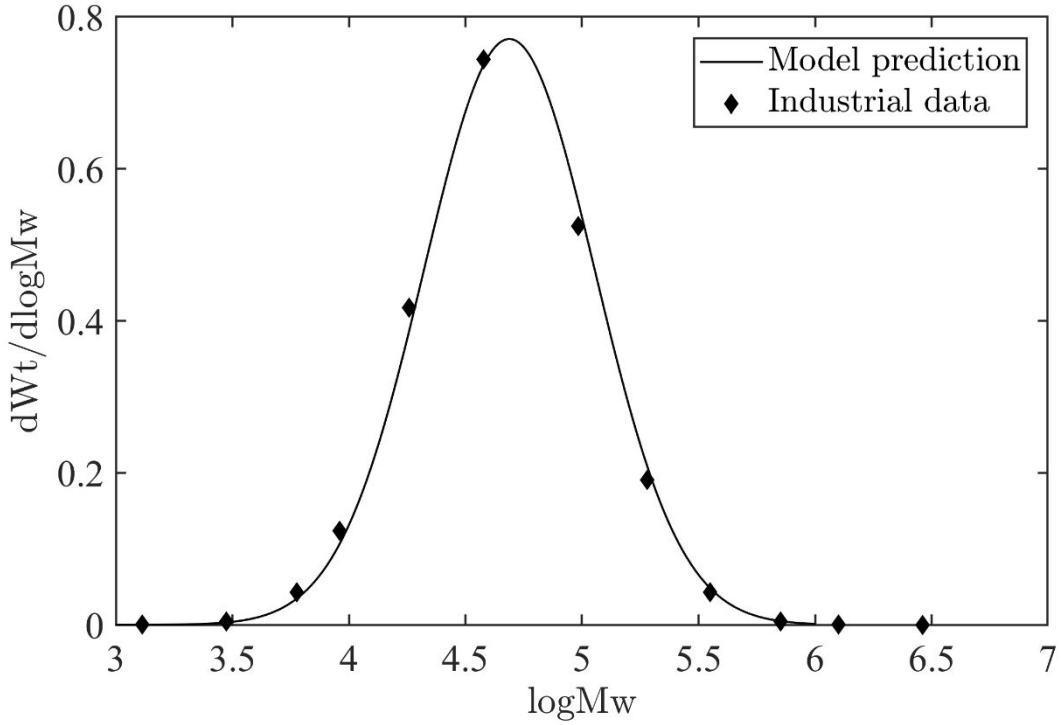

Figure 6: Model predicted molecular weight distribution comparison with industrial data

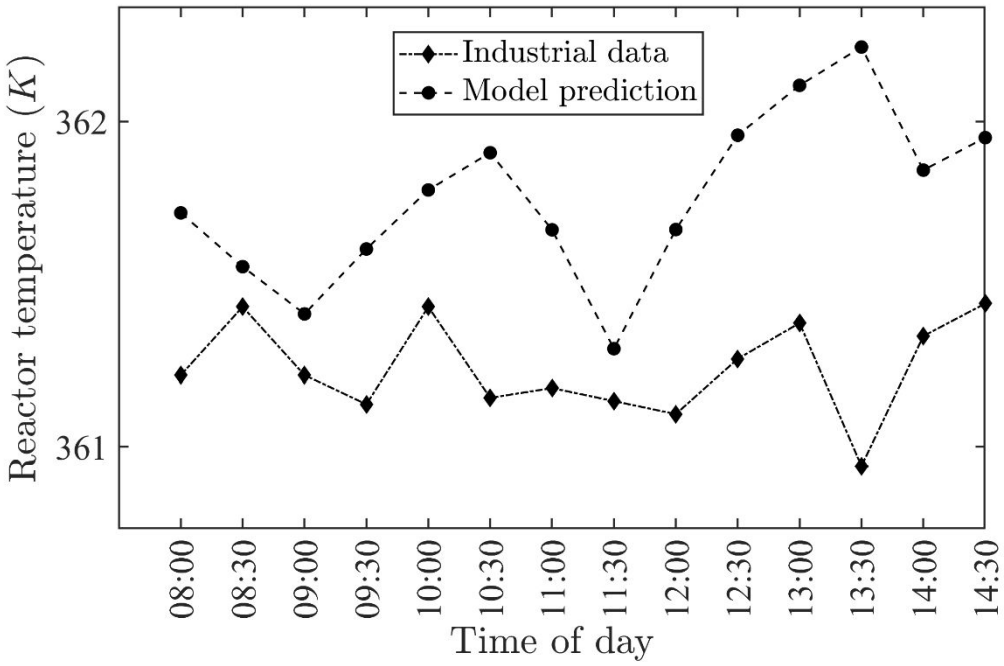

Figure 7: Reactor temperature and industrial data comparison during an operating shift

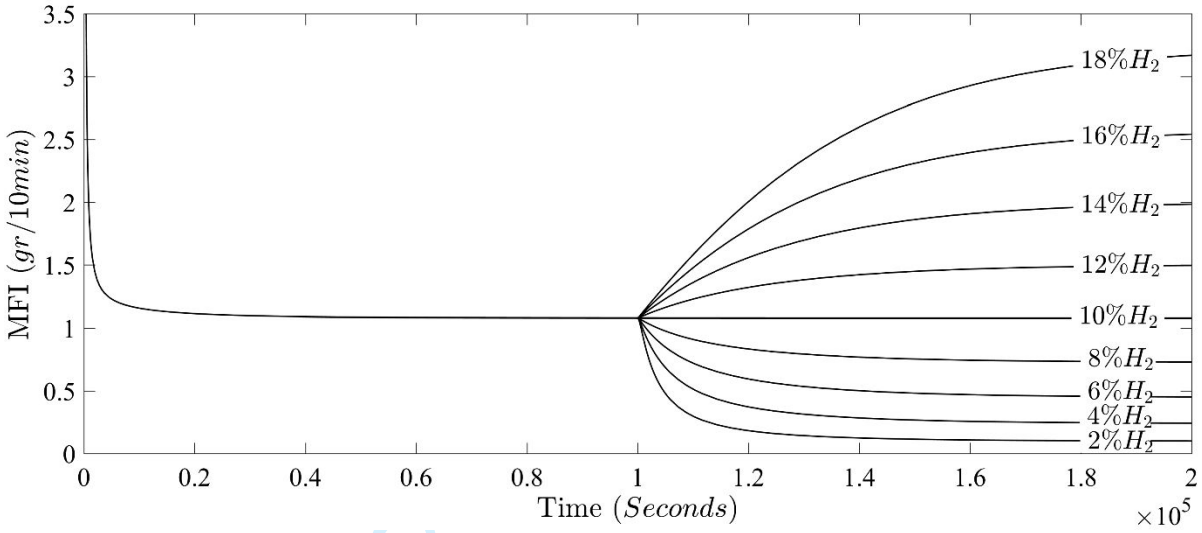

Figure 8: Open loop dynamic response of MFI for different hydrogen inlet concentrations over time

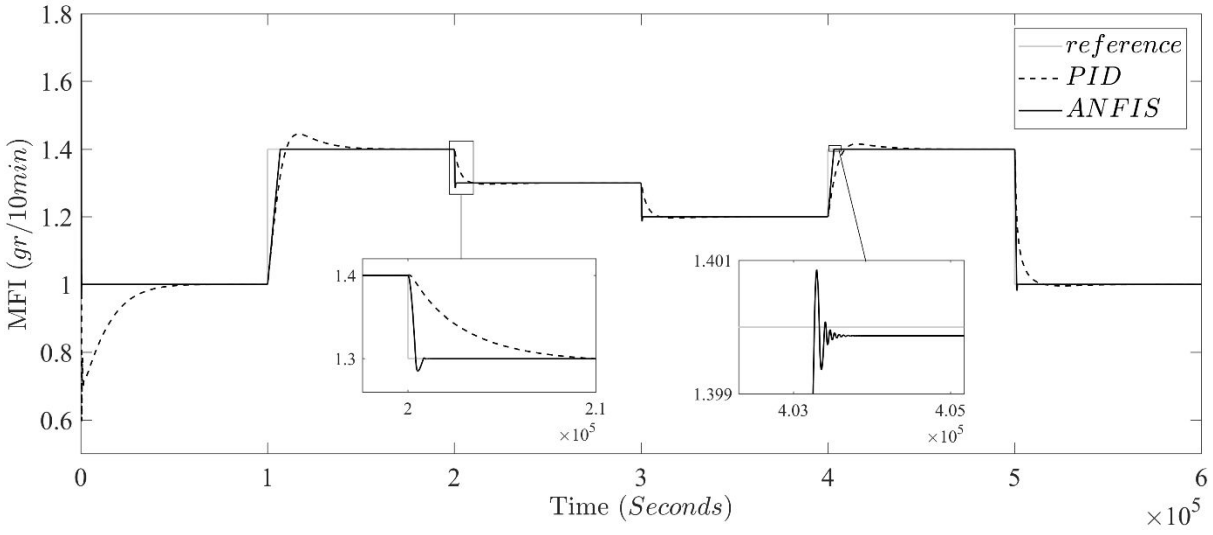

Figure 9: Comparison of MFI reference tracking for PID (P=0.6, I=0.0006, D=-50) and ANFIS controllers

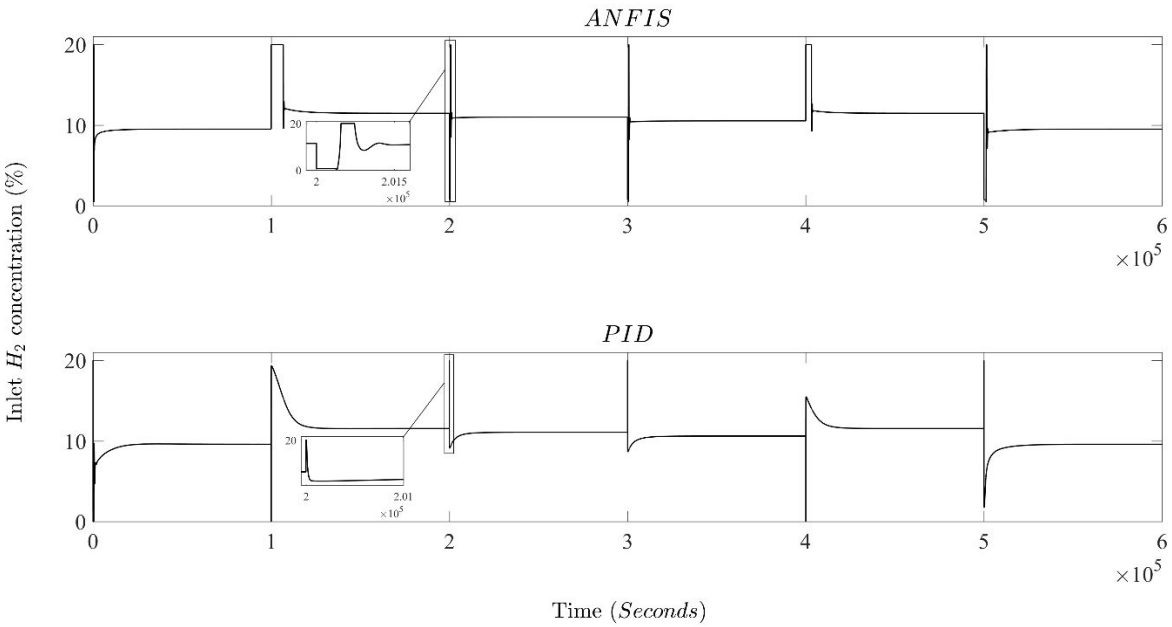

Figure 10: Controller moves in set point tracking of polymer MFI

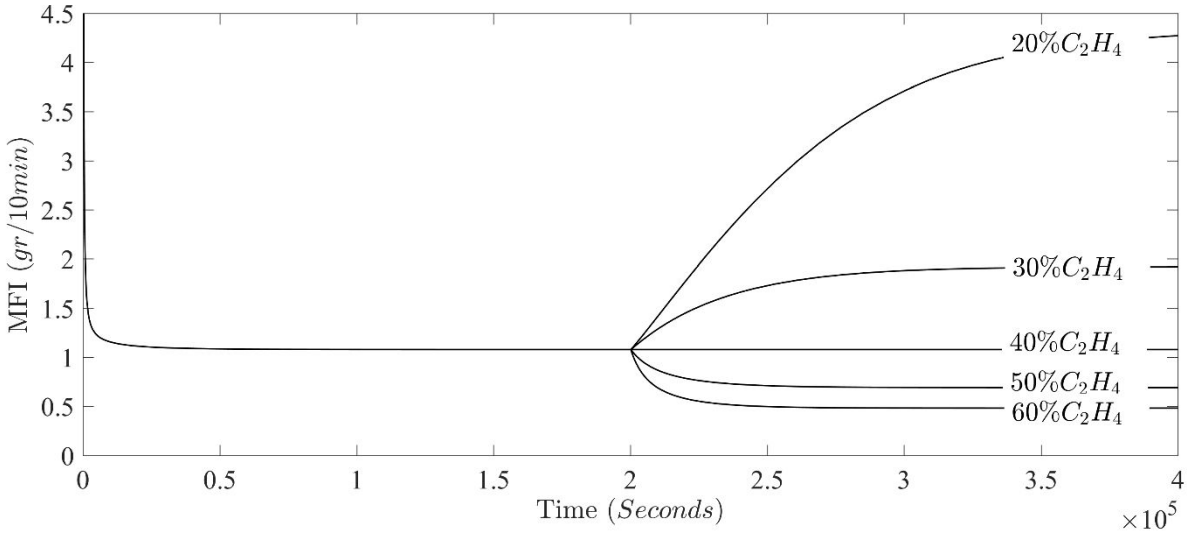

Figure 11: Effect of different inlet ethylene concentration step changes on the polymer MFI at 2×10^5 s

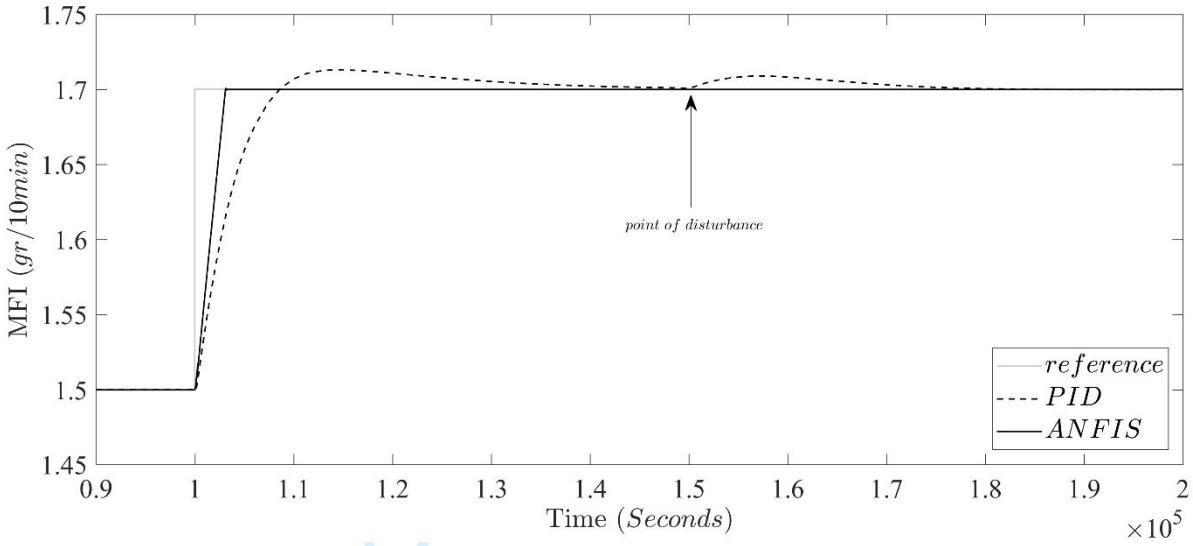

Figure 12: Performance comparison of the controllers in rejecting the effect of a 50% decrease in inlet ethylene concentration on the polymer MFI at 1.5×10^5 s

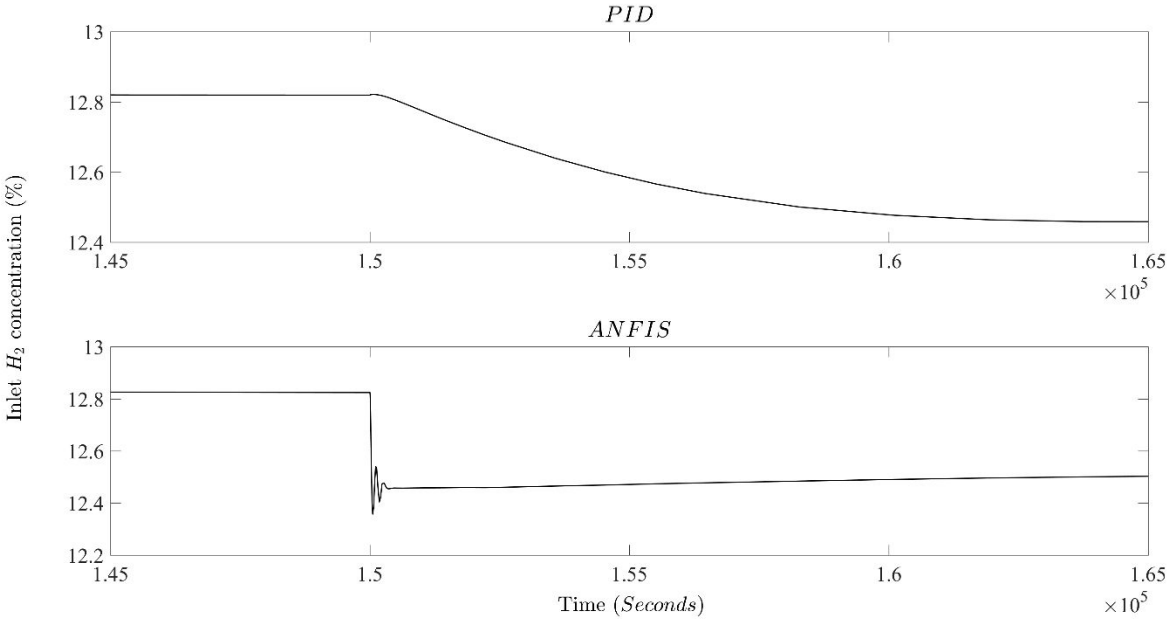

Figure 13: Controller moves in disturbance rejection for a 50% decrease in inlet ethylene concentration on the polymer MFI at $1.5 \times 10^5\ s$

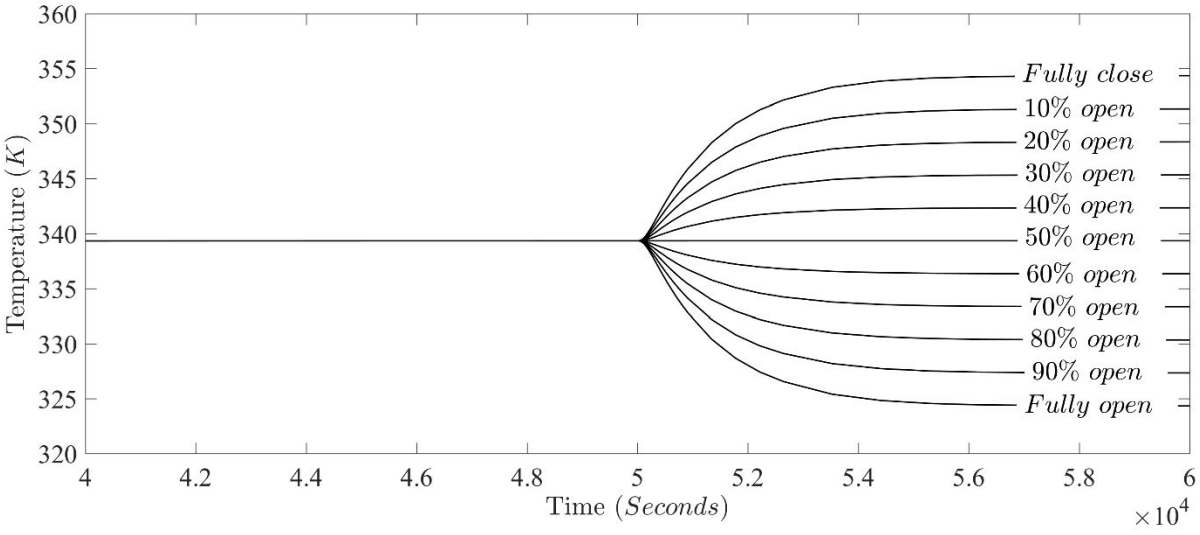

Figure 14: Open loop dynamic response of temperature to different opening percentages of the cool water valve

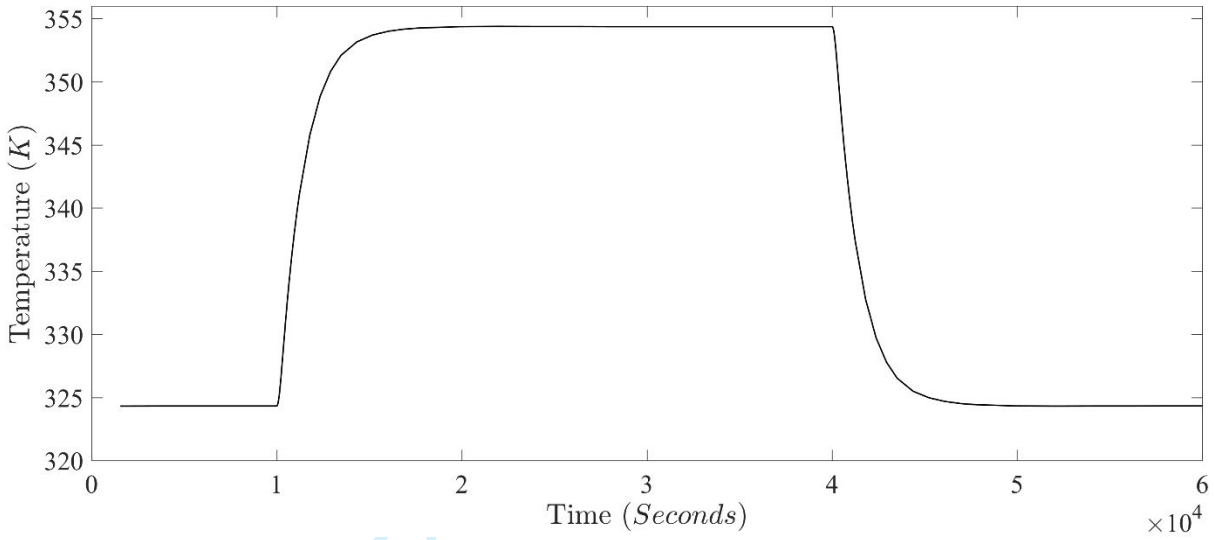

Figure 15: Open loop dynamic response of temperature to fully closing ($1 \times 10^4\ s$) and fully opening ($4 \times 10^4\ s$) of the cool water valve

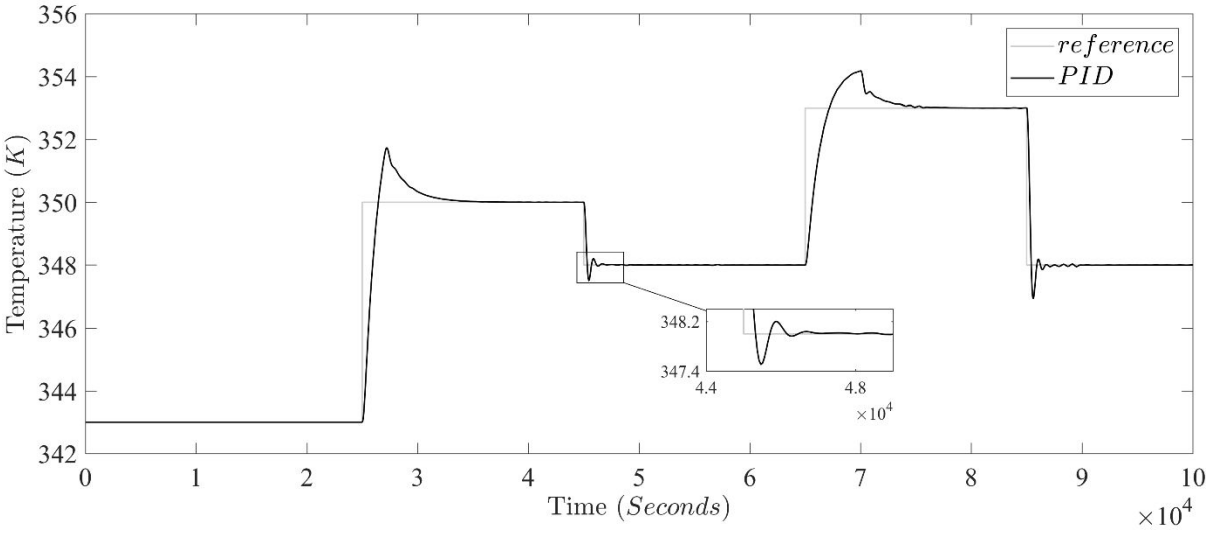

Figure 16: Temperature reference tracking using PID controller (P=-32.61, I=-0.018, D=47.32)

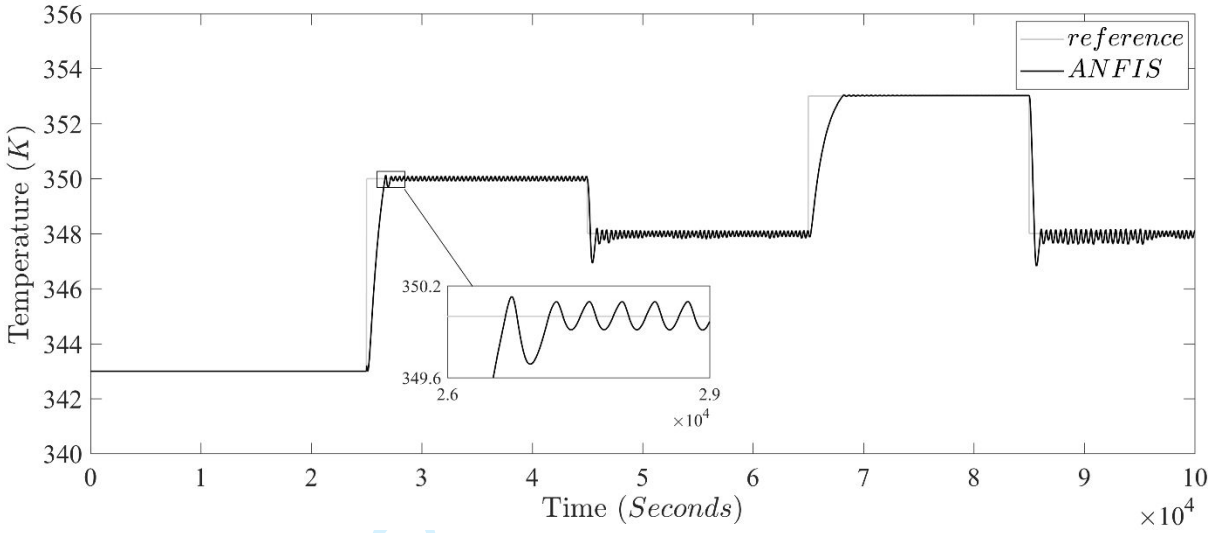

Figure 17: Temperature reference tracking using ANFIS controller

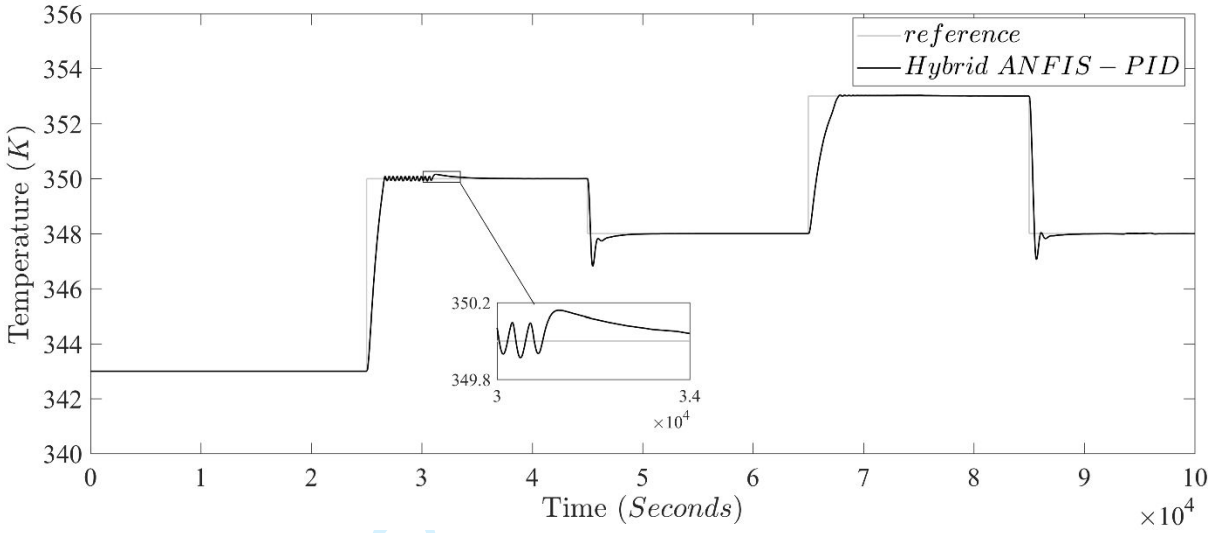

Figure 18: Temperature reference tracking using hybrid ANFIS-PID controller

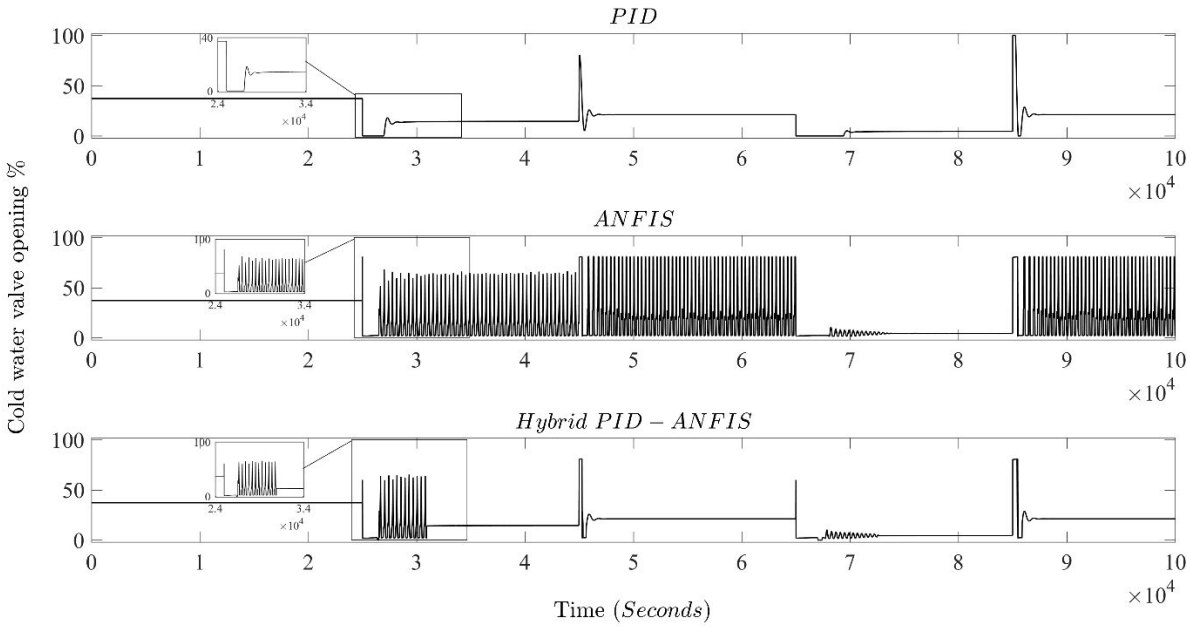

Figure 19: Controller moves in reactor temperature set point tracking

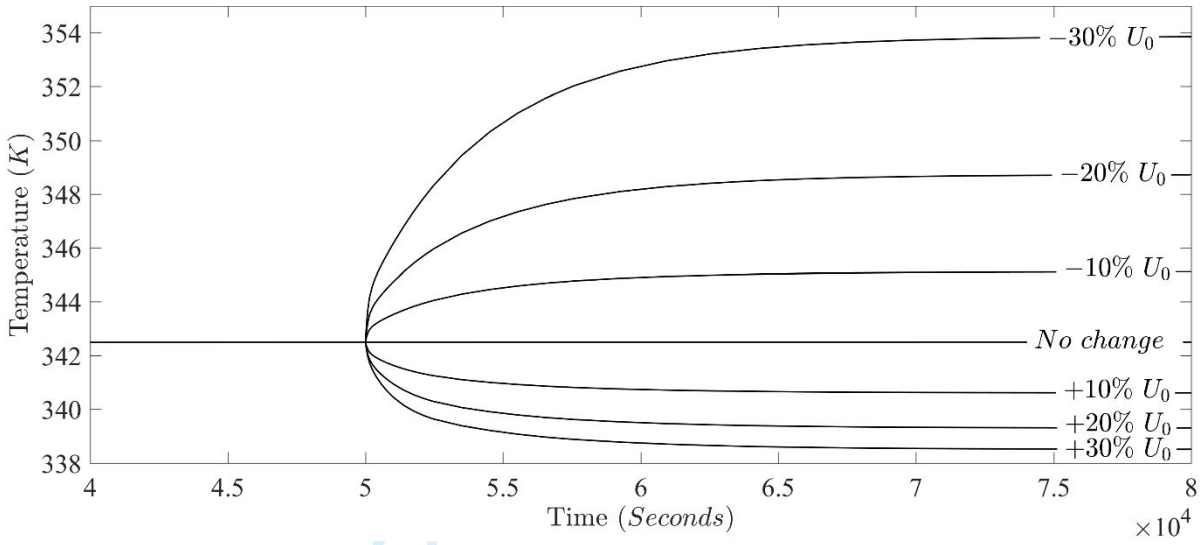

Figure 20: Effect of the superficial gas velocity step changes on the reactor temperature at 5×10^4 s

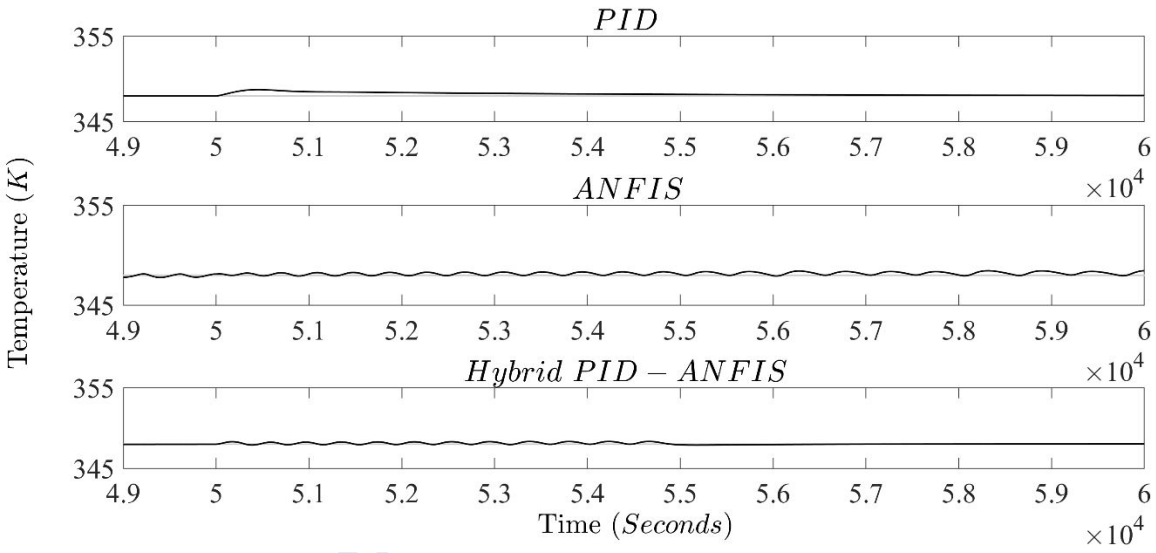

Figure 21: Performance comparison of temperature controllers in rejecting the effect of a 30% decrease in superficial gas velocity at 5×10^4 s

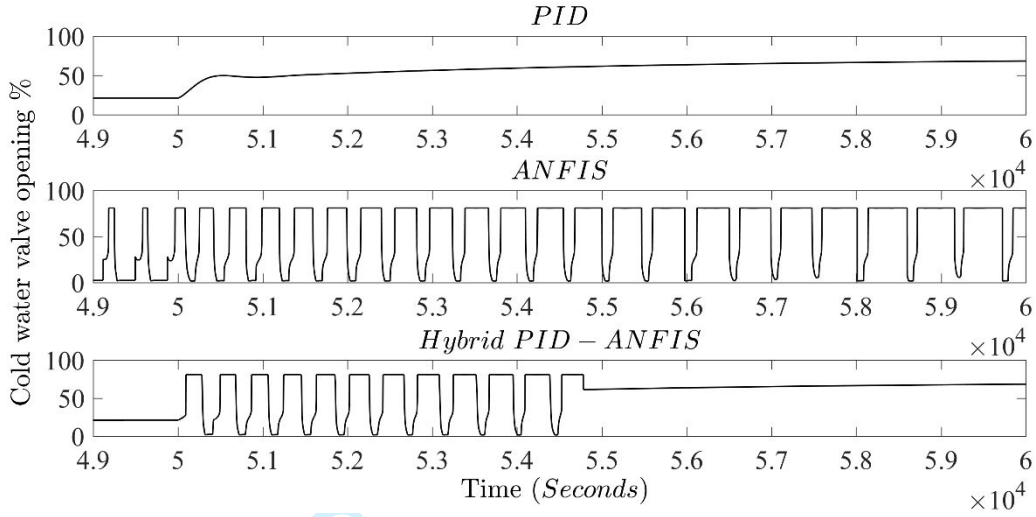

Figure 22: Controller moves in disturbance rejection during temperature control for a 30% decrease in superficial gas velocity at 5×10^4 s

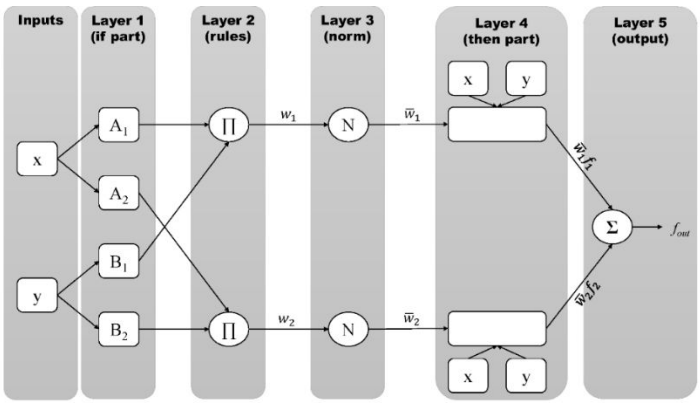

Figure A1: ANFIS structure for two inputs and one output

Table 1: Copolymerization reactions [22]

Description	Reaction
Formation reaction	$N^*(j) \xrightarrow{kf(j)} N(0,j)$
Initiation reaction	$N(0,j) + M_i \xrightarrow{ki_i(j)} N_i(1,j) \quad i = 1,2,..$
Propagation	$N_i(r,j) + M_k \xrightarrow{kp_{ik}(j)} N_k(r+1,j) \quad i = k = 1,2,..$
Transfer to monomer	$N_i(r,j) + M_k \xrightarrow{kfm_{ik}(j)} N_k(1,j) + Q(r,j) \quad i = k = 1,2,..$
Transfer to hydrogen	$N_i(r,j) + H_2 \xrightarrow{kfh_i(j)} N_H(0,j) + Q(r,j) \quad i = 1,2,..$
	$N_H(0,j) + M_i \xrightarrow{kh_i(j)} N_i(1,j) \quad i = 1,2,..$
	$N_H(0,j) + AlEt_3 \xrightarrow{kh_r(j)} N_i(1,j)$
Transfer to co-catalyst	$N_i(r,j) + AlEt_3 \xrightarrow{kfr_i(j)} N_1(1,j) + Q(r,j) \quad i = 1,2,..$
Spontaneous transfer	$N_i(r,j) \xrightarrow{kfs_i(j)} N_H(0,j) + Q(r,j) \quad i = 1,2,..$
Deactivation reactions	$N_i(r,j) \xrightarrow{kds_i(j)} N_d(0,j) + Q(r,j) \quad i = 1,2,..$
	$N(0,j) \xrightarrow{kds(j)} N_d(j)$
	$N_H(0,j) \xrightarrow{kds(j)} N_d(j)$
Reactions with poisons	$N_i(r,j) + I_m \xrightarrow{kdI(j)} N_{dIH}(0,j) + Q(r,j) \quad i = 1,2,..$
	$N_H(0,j) + I_m \xrightarrow{kdI(j)} N_{dIH}(0,j)$
	$N(0,j) + I_m \xrightarrow{kdI(j)} N_{dI}(0,j)$

Table 2: Table 2: Moment equations obtained from Table 1

$$\frac{dY(0,j)}{dt} = [M_T]\left\{k_{i_T}(j)N(0,j) + k_{h_T}(j)N_H(0,j)\right\} + k_{h_r}(j)N_H(0,j)[AlEt_3]$$

$$-Y(0,j)\left\{k_{fh_T}(j)[H_2] + k_{fs_T}(j) + k_{ds}(j) + k_{dI}(j)[I_m] + \frac{R_v}{V_p}\right\}$$

$$\frac{dY(1,j)}{dt} = [M_T]\left\{k_{i_T}(j)N(0,j) + k_{h_T}(j)N_H(0,j)\right\}$$

$$+k_{h_r}(j)N_H(0,j)[AlEt_3] + [M_T]k_{p_{TT}}(j)Y(0,j)$$

$$+\left\{Y(0,j) - Y(1,j)\right\}\left\{k_{fm_{TT}}(j)[M_T] + k_{fr_T}(j)[AlEt_3]\right\}$$

$$-Y(1,j)\left\{k_{fh_T}(j)[H_2] + k_{fs_T}(j) + k_{ds}(j) + k_{dI}(j)[I_m] + \frac{R_v}{V_p}\right\}$$

$$\frac{dY(2,j)}{dt} = [M_T]\left\{k_{i_T}(j)N(0,j) + k_{h_T}(j)N_H(0,j)\right\}$$

$$+k_{h_r}(j)N_H(0,j)[AlEt_3] + [M_T]k_{p_{TT}}(j)\left\{2Y(1,j) - Y(0,j)\right\}$$

$$+\left\{Y(0,j) - Y(2,j)\right\}\left\{k_{fm_{TT}}(j)[M_T] + k_{fr_T}(j)[AlEt_3]\right\}$$

$$-Y(2,j)\left\{k_{fh_T}(j)[H_2] + k_{fs_T}(j) + k_{ds}(j) + k_{dI}(j)[I_m] + \frac{R_v}{V_p}\right\}$$

$$\frac{dX(n,j)}{dt} = \left\{k_{fm_{TT}}(j)[M_T] + k_{fr_T}(j)[AlEt_3] + k_{fh_T}(j)[H_2] + k_{fs_T}(j) + k_{ds}(j) + k_d I(j)[I_m]\right\}$$

$$\left\{Y(n,j) - N_T(1,j)\right\} - X(n,j)\frac{R_v}{V_p} \quad n = 0,1,2$$

Table 3: Reaction rate constants of two-site ethylene copolymerization [22]

Reaction	Rate constant	Unit	Site type 1	Site type 2
Formation	$k_f(j)$	s^{-1}	1	1
Initiation	$k_{i_1}(j)$	L/kmol s	1	1
	$k_{i_2}(j)$	L/kmol s	0.14	0.14
	$k_{h_1}(j)$	L/kmol s	1	1
	$k_{h_2}(j)$	L/kmol s	0.1	0.1
	$k_{h_r}(j)$	L/kmol s	20	20
Propagation	$k_{p_{11}}(j)$	L/kmol s	85	85
	$k_{p_{12}}(j)$	L/kmol s	2	15
	$k_{p_{21}}(j)$	L/kmol s	64	64
	$k_{p_{22}}(j)$	L/kmol s	1.5	6.2
Transfer	$k_{fm_{11}}(j)$	L/kmol s	0.0021	0.0021
	$k_{fm_{12}}(j)$	L/kmol s	0.006	0.11
	$k_{fm_{21}}(j)$	L/kmol s	0.0021	0.001
	$k_{fm_{22}}(j)$	L/kmol s	0.006	0.11
	$k_{fh_1}(j)$	L/kmol s	0.088	0.37
	$k_{fh_2}(j)$	L/kmol s	0.088	0.37
	$k_{fr_1}(j)$	L/kmol s	0.024	0.12
	$k_{fr_2}(j)$	L/kmol s	0.048	0.24
	$k_{fs_1}(j)$	L/kmol s	0.0001	0.0001
	$k_{fs_2}(j)$	L/kmol s	0.0001	0.0001
Deactivation	$k_{ds}(j)$	s^{-1}	0.0001	0.0001
	$k_{dI}(j)$	L/kmol s	2000	2000
Impurity	$k_a(j)$	s^{-1}	0.0003	0.0003

Table 4: Hydrodynamic equations

Parameter	Formula	Reference
Minimum fluidization velocity	$\mathrm{Re}_{mf} = [29.5^2 + 0.375Ar]^{0.5} - 29.5$	32
Bubble velocity	$U_b = U_0 - U_{mf} + U_{br}$	33
Bubble rise velocity	$U_{br} = 0.711(\mathrm{g}\mathrm{d}_b)^{0.5}$	33
Emulsion velocity	$U_e = \dfrac{U_0 - U_b}{(1-\delta)}$	34
Bubble diameter	$d_b = d_{b0}\left[1 + 27(U_0 - U_e\right]^{0.33}\left(1 + 6.84H\right)$ $d_{b0} = 0.0085(\,for\ GeldartB)$	35
Mass transfer coefficient	$k_{be} = \left(\dfrac{1}{k_{bc}} + \dfrac{1}{k_{ce}}\right)^{-1}$ $K_{bc} = 4.5\left(\dfrac{U_e}{d_b}\right) + 5.85\left(\dfrac{D_g^{0.5} g^{0.25}}{d_b^{1.25}}\right)$ $K_{ce} = 6.77\left(\dfrac{D_g \varepsilon_e U_{br}}{d_b}\right)$	33
Heat transfer coefficient	$H_{be} = \left(\dfrac{1}{H_{bc}} + \dfrac{1}{H_{ce}}\right)^{-1}$ $H_{bc} = 4.5\left(\dfrac{U_e \rho_g C_{pg}}{d_b}\right) + 5.85\dfrac{\left(k_g \rho_g C_{pg}\right)^{0.5} g^{0.25}}{d_b^{1.25}}$ $H_{ce} = 6.77\left(\rho_g C_{pg} k_g\right)^{0.5}\left(\dfrac{\varepsilon_e U_{br}}{3}\right)^{0.5}$	33
Bubble phase fraction Emulsion	$\delta = 0.534\left[1 - exp\left(\dfrac{U_0 - U_{mf}}{0.413}\right)\right]$	36
Emulsion phase porosity	$\varepsilon_e = \varepsilon_{mf} + 0.2 - 0.059\exp\left(-\dfrac{U_0 - U_{mf}}{0.429}\right)$	36
Bubble phase porosity	$\varepsilon_b = 1 - 0.146\exp\left(-\dfrac{U_0 - U_{mf}}{4.439}\right)$	36
Volume of polymer phase in the emulsion phase	$V_{Pe} = AH(1-\varepsilon_e)(1-\delta)$	37
Volume of polymer phase in the bubble phase	$V_{Pb} = AH(1-\varepsilon_b)\delta$	37
Volume of the emulsion phase	$V_e = A\left(1-\delta\right)H$	37
Volume of the bubble phase	$V_b = A\delta H$	37

Table 5: Mass and energy balances attained by considering the assumptions

Type	Equation
Mass balance (emulsion)	$\frac{d}{dt}(V_e\varepsilon_e[M_i]_e) = [M_i]_{e,(in)}U_eA_e - [M_i]_eU_eA_e - R_v\varepsilon_e[M_i]_e$ $+K_{be}\left([M_i]_b - [M_i]_e\right)V_e\left(\frac{\delta}{1-\delta}\right) - (1-\varepsilon_e)R_{ie} - \frac{K_eV_e\varepsilon_eA_e[M_i]_e}{W_e}$
Mass balance (bubble)	$\frac{d}{dt}(V_b\varepsilon_b[M_i]_b) = [M_i]_{b,(in)}U_bA_b - [M_i]_bU_bA_b - R_v\varepsilon_b[M_i]_b$ $-K_{be}\left([M_i]_b - [M_i]_e\right)V_b - (1-\varepsilon_b)\frac{A_b}{V_{PFR}}\int R_{ib}dz - \frac{K_eV_e\varepsilon_eA_e[M_i]_e}{W_e}$
Energy balance (emulsion)	$U_eA_e\left(T_{e.(in)} - T_{ref}\right)\sum_{i=1}^{m}[M_i]_{e,(in)}C_{pi} - U_eA_e\left(T_e - T_{ref}\right)\sum_{i=1}^{m}[M_i]_eC_{pi}$ $-R_v(T_e - T_{ref})\left(\sum_{i=1}^{m}\varepsilon_eC_{pi}[M_i]_e + (1-\varepsilon_b)\rho_{pol}C_{p.pol}\right)$ $+(1-\varepsilon_e)R_{pe}\Delta H_R - H_{be}V_e\left(\frac{\delta}{1-\delta}\right)(T_e - T_b)$ $-V_e\varepsilon_e\left(T_e - T_{ref}\right)\sum_{i=1}^{m}C_{pi}\frac{d}{dt}\left([M_i]_e\right)$ $-\frac{K_eA_e}{W_e}\left(T_e - T_{ref}\right)\left(\sum_{i=1}^{m}\varepsilon_eC_{pi}[M_i]_e + (1-\varepsilon_b)\rho_{pol}C_{p.pol}\right)$ $= V_e\left(\varepsilon_e\sum_{i=1}^{m}C_{pi}[M_i]_e + (1-\varepsilon_e)\rho_{pol}C_{p.pol}\right)\frac{d}{dt}\left(T_e - T_{ref}\right)$
Energy balance (bubble)	$U_bA_b\left(T_{b.(in)} - T_{ref}\right)\sum_{i=1}^{m}[M_i]_{b,(in)}C_{pi} - U_bA_b\left(T_b - T_{ref}\right)\sum_{i=1}^{m}[M_i]_bC_{pi}$ $-R_v\left(T_b - T_{ref}\right)\left(\sum_{i=1}^{m}\varepsilon_bC_{pi}[M_i]_b + (1-\varepsilon_e)\rho_{pol}C_{p.pol}\right)$ $+(1-\varepsilon_b)\frac{A_b\Delta H_R}{V_{PFR}}\int R_{pb}dz + H_{be}V_b\left(T_e - T\right)_b$ $-V_b\varepsilon_b\left(T_b - T_{ref}\right)\sum_{i=1}^{m}C_{pi}\frac{d}{dt}\left([M_i]_b\right)$ $-\frac{K_bA_b}{W_b}\left(T_b - T_{ref}\right)\left(\sum_{i=1}^{m}\varepsilon_bC_{pi}[M_i]_b + (1-\varepsilon_b)\rho_{pol}C_{p.pol}\right)$ $= \left(V_b\left(\varepsilon_b\sum_{i=1}^{m}C_{pi}[M_i]_b + (1-\varepsilon_b)\rho_{pol}C_{p.pol}\right)\right)\frac{d}{dt}\left(T_b - T_{ref}\right)$

Table 6: Solids elutriation equations used in the model

Parameter	Formula	Referenc
Elutriation rate constant in emulsion phase	$K_e = 23.7\rho_g U_0 \frac{A}{W_e} exp\left(\frac{-5.4U_t}{U_0}\right)$	38
Elutriation rate constant in bubble phase	$K_b = 23.7\rho_g U_0 \frac{A}{W_b} exp\left(\frac{-5.4U_t}{U_0}\right)$	38
Weight of solids in the emulsion phase	$W_e = AH\left(1-\varepsilon_e\right)\rho_{pol}$	33
Weight of solids in the bubble phase	$W_b = AH\left(1-\varepsilon_b\right)\rho_{pol}$	33
Terminal velocity of falling particles	$U_t = \frac{U_t^*}{\left[\mu\rho_g^{-2}\left(\rho_{pol}-\rho_g\right)g\right]^{0.33}}$	39
Dimensionless terminal falling velocity coefficien	$U_t^* = \left[18\left(d_p^*\right)^{-2} + \left(2.335-1.744\varnothing_s\right)\left(d_p^*\right)^{-0.5}\right]^{-1}$	39
dimensionless particle size	$d_p^* = d_p\left[\mu_g^{-2}\rho_g\left(\rho_{pol}-\rho_g\right)g\right]^{0.33} \quad for \quad 0.5 < \varnothing_s \leq 1$	39

Table 7: Specifications of the developed ANFIS structures for MFI and temperature control

Parameter	MFI ANFIS	Temperature ANFIS
Fuzzy structure	Sugeno	Sugeno
Membership function type	Triangular	Gaussian
Number of inputs	2	2
Number of outputs	1	1
Optimization method	Hybrid (least square and back propagation technique)	Hybrid (least square and back propagation technique)
Number of fuzzy rules	9	25

Table 8: Performance indexes for MFI controllers

	Setpoint tracking		Disturbance rejection	
	PID	ANFIS	PID	ANFIS
ITAE	1.44×10^{9}	4.38×10^{8}	2.13×10^{9}	6.52×10^{8}
IAE	9826	2390	1.16×10^{4}	2886
ISE	1748	771.6	1911	870.4
APE	8687	1879	1.01×10^{4}	2302

Table 9: Performance indexes for temperature controllers

	Setpoint tracking			Disturbance rejection		
	PID	ANFIS	Hybrid	PID	ANFIS	Hybrid
ITAE	1.53×10^{9}	1.08×10^{9}	9.81×10^{8}	1.59×10^{9}	1.63×10^{9}	1.16×10^{9}
IAE	1.14×10^{5}	6.98×10^{4}	6.67×10^{4}	1.14×10^{5}	7.62×10^{4}	6.91×10^{4}
ISE	1.01×10^{6}	7.80×10^{5}	7.82×10^{5}	7.83×10^{5}	7.83×10^{5}	7.79×10^{5}
APE	3.31×10^{2}	2.03×10^{2}	1.93×10^{2}	3.34×10^{1}	2.21×10^{2}	2.01×10^{2}